MARKOV RANDOM FIELD BASED ROAD NETWORK EXTRACTION FROM HIGH RESOULUTION SATELLITE IMAGES

A THESIS SUBMITTED TO
THE GRADUATE SCHOOL OF NATURAL AND APPLIED SCIENCES
OF
MIDDLE EAST TECHNICAL UNIVERSITY

BY

MAHİR ÖZTÜRK

IN PARTIAL FULLFILLMENT OF THE REQUIREMENTS
FOR
THE DEGREE OF MASTER OF SCIENCE
IN
ELECTRICAL AND ELECTRONICS ENGINEERING

JANUARY 2013

Approval of the thesis:

MARKOV RANDOM FIELD BASED ROAD NETWORK EXTRACTION FROM HIGH RESOULUTION SATELLITE IMAGES

submitted by **MAHİR ÖZTÜRK** in partial fulfillment of the requirements for the degree of **Master of Science in Electrical and Electronics Engineering Department, Middle East Technical University** by,

Prof. Dr. Canan Özgen
Dean, Graduate School of **Natural and Applied Sciences** _____

Prof. Dr. İsmet Erkmen
Head of Department, **Electrical and Electronics Engineering** _____

Prof. Dr. Uğur Halıcı
Supervisor, **Electrical and Electronics Engineering Dept., METU** _____

Examining Committee Members

Prof. Dr. A. Aydın Alatan
Electrical and Electronics Engineering Dept., METU _____

Prof. Dr. Uğur Halıcı
Electrical and Electronics Engineering Dept., METU _____

Prof. Dr. Gözde B. Akar
Electrical and Electronics Engineering Dept., METU _____

Assoc. Prof. Dr. İlkay Ulusoy
Electrical and Electronics Engineering Dept., METU _____

Barış Konuk, M.Sc.
ASELSAN Inc. _____

Date: 31.01.2013

I hereby declare that all information in this document has been obtained and presented in accordance with academic rules and ethical conduct. I also declare that, as required by these rules and conduct, I have fully cited and referenced all material and results that are not original to this work.

Name, Last name : Mahir Öztürk

Signature :

ABSTRACT

MARKOV RANDOM FIELD BASED ROAD NETWORK EXTRACTION FROM HIGH RESOLUTION SATELLITE IMAGES

Öztürk, Mahir
M.S., Department of Electrical and Electronics Engineering
Supervisor : Prof. Dr. Uğur Halıcı

January 2013, 76 pages

Road Networks play an important role in various applications such as urban and rural planning, infrastructure planning, transportation management, vehicle navigation. Extraction of Roads from Remote Sensed satellite images for updating road database in geographical information systems (GIS) is generally done manually by a human operator. However, manual extraction of roads is time consuming and labor intensive process. In the existing literature, there are a great number of researches published for the purpose of automating the road extraction process. However, automated processes still yield some erroneous and incomplete results and human intervention is still required.

The aim of this research is to propose a framework for road network extraction from high spatial resolution multi-spectral imagery (MSI) to improve the accuracy of road extraction systems. The proposed framework begins with a spectral classification using One-class Support Vector Machines (SVM) and Gaussian Mixture Models (GMM) classifiers. Spectral Classification exploits the spectral signature of road surfaces to classify road pixels. Then, an iterative template matching filter is proposed to refine spectral classification results. K-medians clustering algorithm is employed to detect candidate road centerline points. Final road network formation is achieved by Markov Random Fields. The extracted road network is evaluated against a reference dataset using a set of quality metrics.

Keywords: Road extraction, satellite images, One-class Support Vector Machines, Gaussian Mixture Models, Template-matching filter, K-medians clustering, Markov Random Fields,

ÖZ

YÜKSEK ÇÖZÜNÜRLÜKLÜ UYDU GÖRÜNTÜLERİNDEN MARKOV RASTGELE ALAN BAZLI YOL AĞI ÇIKARIMI

Öztürk, Mahir
Yüksek Lisans, Elektrik-Elektronik Mühendisliği Bölümü
Tez Yöneticisi : Prof. Dr. Uğur Halıcı

Ocak 2013, 76 sayfa

Yol Ağları kırsal ve kentsel planlama, altyapı planlaması, taşımacılık yönetimi, araç navigasyon sistemleri gibi çeşitli uygulamalarda önemli bir rol oynamaktadır. Coğrafi Bilgi Sistemleri'nin (CBS) yol veritabanı güncellenmesi genellikle uygu görüntülerinden yolların manuel çıkarımı ile yapılmaktadır. Ancak bu işlem zaman alıcı ve yoğun emek gerektiren bir süreçtir. Mevcut literatürde, yolları çıkarımı işlemini otomatikleştirme amacıyla yayınlanmış çok sayıda araştırma vardır. Ancak, otomatik işlemler bazı hatalı ve eksik sonuçlar üretmekte ve hala insan müdahalesini zorunlu kılmaktadır.

Bu araştırmanın amacı, yüksek çözünürlüklü multi-spektral uydu görüntülerden yol ağının çıkarılması için bir yöntem önererek varolan yöntemlerin doğruluğunu geliştirmektir. Önerilen yöntem Tek Sınıf Destek Vektör Makineleri ve Gauss Karışım Modelleri sınıflandırıcıları kullanarak görüntülerin spektral sınıflandırılması ile başlar. Daha sonra sınıflandırma işleminin sonuçlarını iyileştirmek amacıyla önerilen iteratif şablon eşleme filtresi uygulanır. K-medyan kümeleme algoritması ile çıkarılan muhtemel yolların orta noktaları tespit edilir. Nihai yol ağı Markof Rasgele Alanı yöntemi kullanılarak çıkartılır. Yol çıkarım algorithmasının sonuçları bir dizi kalite metrikleri kullanılarak değerlendirilmiştir.

Anahtar Kelimeler: Yol çıkarımı, uydu görüntüleri, Tek Sınıf Destek Vektör Makineleri, Gauss Karışım Modelleri, Şablon eşleştirme filtresi, K-medyan kümeleme, Markof Rastgele Alanlar,

To My Family

ACKNOWLEDGEMENTS

I would like to sincere thanks and gratitude to my supervisor Prof. Dr. Uğur HALICI for her valuable guidance and opinions they provided throughout my research.

I would like to express my thanks to my friends for their support and fellowship.

Finally, I would like to give special thanks to my family for their endless support, love and encouragements.

TABLE OF CONTENTS

LIST OF TABLES

TABLES

LIST OF FIGURES

FIGURES

LIST OF ABBREVIATIONS

ACE	Anti-parallel-edge Centerline Extraction
APAR	Anti-Parallel
CV	Cross-Validation
CVA	Cross Validation Accuracy
EM	Expectation Maximization
FDS	Fraction of Decision Space
FO	Fraction of Outliers
FSV	Fraction of Support Vector
GIS	Geographical Information System
GMM	Gaussian Mixture Model
HSI	Hue Saturation Intensity
ICM	Iterated Conditional Modes
ISODATA	Iterative Self-Organizing Data Analysis Technique
MAP	Maximum a Posteriori Probability
ML	Maximum Likelihood
MRF	Markov Random Field
MSI	Multi-Spectral Imagery
MST	Minimum Spanning Tree
NIR	Near Infrared
OC-SVM	One-class Support Vector Machines
PC	Principal Components
PCA	Principal Component Analysis
RAG	Region Adjacency Graph
RGB	Red Green Blue
RJMCMC	Reversible Jump Monte Carlo Markov Chain
RMSE	Root Mean Square Error
RNE	Road Network Extraction
SAR	Synthetic Aperture Radar
SOM	Self-Organizing Map
SORM	Self-Organized Road Map
SVM	Support Vector Machine
TMF	Template Matching Filter

CHAPTER 1

INTRODUCTION

1.1 Motivation

The extraction of geospatial objects from remotely sensed imagery has a great importance in many practical applications. Most of the studies on road extraction are mainly motivated by importance of geospatial information systems. GIS is a system capable of capturing, managing, analyzing and displaying various types of geographical data. Road Networks are a vital part of GIS applications such as urban and rural planning, vehicle navigation, transportation management, etc. Road maps are generally delineated manually by human operators. However, manual extraction of roads is time consuming and labor intensive work. So automating the extraction process will reduce extraction times and also the cost of creating or updating maps.

1.2 Literature Survey

There are a great number of techniques available in literature aimed to detect roads from remotely sensed images. Road Extraction methods are categorized by Mena (2003) in which more than 250 different studies are reviewed. Different methods are first grouped into various categories, according to technique and level of processing. These techniques are generally trying to extract road mask or road network. In the literature survey presented in this thesis, the main focus lies on road network extraction techniques. First road classification then road centerline extraction and finally road network formation related studies are presented.

1.2.1 Road Classification

Classification used in road extractions systems generally exploits spectral signature of roads. However, the main difficulty lies in the high misclassification between roads and other spectrally similar objects, such as parking lots, buildings, crop fields, etc. In the literature, other features such as textural, geometrical and contextual features are also employed for classification.

Mena & Malpica (2005) applied texture statistics method for automatic road extraction in rural and semi-urban areas. They conducted binary segmentation based on three levels of texture statistics. Dempster-Shafer fusion is used to combine these results. Finally the obtained binary image was vectorized by skeleton extraction and morphological operators.

Song & Civco (2004) employed the support vector machine (SVM) to classify IKONOS imagery into a road group and a non-road group using spectral features. Road group pixels were segmented into geometrically homogeneous objects using a region growing technique based on a similarity criterion considering shape and spectral features of objects. A simple thresholding on the shape and density features of these objects was performed to remove the most of the false-roads objects, which were further processed by thinning and vectorization to obtain road centerlines.

Zhang (2004) used ISODATA clustering algorithm to segment and classify images into five classes: road regions, vegetation, shadow areas, dark roofs and red roofs. Instead of raw spectral bands (Red, Green and Blue), transformed spectral bands were used. These bands were 1) the first principal component image, 2) a greenness band formed by $(G-R)/(G+R)$, and 3) the saturation component of image data in Hue Saturation Intensity (HSI) color space.

Hinz & Baumgartner (2003) performed automatic extraction of urban road networks from multi-view aerial imagery. They used a road model exploiting both global (such as forest, rural or urban areas) and local (such as buildings, cars and road markings) contextual information of roads.

1.2.2 Road centerline extraction

There are a number of road centerline extraction algorithms that can be applied to high resolution classified imagery besides morphological operators such as thinning, skeleton extraction, etc.

A self-organizing road map (SORM) algorithm inspired from the neural network model called Self-Organizing Map (SOM) (2001) is presented by Doucette et al. (2001) for robust centerline extraction from classified images. A minimum spanning tree based linking algorithm is used to derive a consistent network topology from extracted centerline points.

Doucette et al. (2004) present an approach for detecting road centerlines automatically through parallel edge detection. The ACE algorithm follows more stringent criteria when selecting parallel edges. As a road depicted as either brighter or darker than the non-road area, only road edges with opposing gradients are considered. Provisional centerline road seeds are placed halfway between the edges.

Hu et al. (2004) use an iterative Hough transform to detect and extract grid structured road networks from LIDAR data using both the intensity and height information. The color imagery is used to separate grassland and trees from open areas.

1.2.3 Road network formation

Road network formation enables the link between road objects to construct a meaningful road topology. It usually integrates a set of processes including bridging gaps between road segments, creating nodes for road intersections, and removing small branches.

Tupin et al. (1998) presents a method where both local and global techniques for linear feature extractions are combined. In the first part of their algorithm, a local detection of linear features based on the fusion of information from two line detectors is performed. In the second part, a Markov random field (MRF) is defined on a set of candidate segments which introduces contextual knowledge about the shape of the road objects.

Katartzis et al. (2001) presented a model-based approach that combined both geometric and radiometric properties of the linear features they aimed to extract. Their approach consists of two steps. In the local analysis step, a set of morphological operators is used to detect elongated structures. In the global analysis step, a segment linking process is performed based on the MRF framework of Tupin et al (1998).

Géraud & Mouret (2004) are proposed a fast road network extraction system in gray scale satellite imagery. They applied a watershed transform to segment curvilinear objects. The resulting watershed lines are used to build a region adjacency graph (RAG). Then a Markov Random Field (MRF) is defined on this graph and final network construction is handled by a Markovian relaxation.

A road extraction technique using a probabilistic model in the form of a Gibbs point process framework is proposed by Stoica, Descombes and Zerubi (2004). The road network is modeled as connected line segments. The estimate for the network is solved by the Maximum a Posteriori (MAP) estimation using a simulated annealing algorithm based on a Reversible Jump Monte Carlo Markov Chain dynamics (RJMCMC).

Lacoste et al. (2005) provides an extension of the model proposed in Stoica, Descombes and Zerubia (2004), called the “Quality Candy” model, which provides a better model for the curvature, the junctions, and the intersections of the network.

1.3 The Objective and Scope of Thesis

The aim of this thesis is to propose an automatic road network extraction algorithm which is intended to work on high resolution multi-spectral optical images. These images have a spatial resolution of 1 meter and contain 3 (Red, Green, Blue) or 4 (Red, Green, Blue, Near Infrared) spectral bands.

1.4 Contribution of this Thesis

The main contributions of this thesis can be summarized as:

- A complete road network extraction system is presented. Several modifications are proposed in order to improve overall performance of the system.
- An iterative template matching filter is proposed to increase classification accuracy of roads.
- An automatic method to find optimum parameter set for one-class Support Vector Machine (OC-SVM) and Gaussian Mixture Models (GMM) classifiers are presented.
- Original MRF Energy function proposed by Tupin et al. has been modified in order to increase overall network extraction performance.

1.5 Outline of Thesis

The thesis is structured as follows. In Chapter 2, a brief overview of fundamental concepts and background information related to proposed extraction system is covered.

Chapter 3 describes the algorithm blocks used in this study and how they are integrated into a complete road network extraction system. The details of the proposed template matching filter and the modified MRF energy function are given.

In Chapter 4, Quality metrics in order to assess the accuracy of results produced by the proposed framework is provided. Then the performance evaluation of overall system based on these metrics is presented.

Finally, Conclusions and a discussion on future work are provided in Chapter 5.

CHAPTER 2

BACKGROUND

In this chapter, background information about the techniques used in this research is covered. Sections 2.1 and 2.2 will focus on two different classification methods, One-class SVM (OCSVM) and Gaussian Mixture Models (GMM) respectively. Anti-parallel Centerline Extraction (ACE) method will be provided in 2.3. Principal Component Analysis technique is explained in Section 0. Section 2.5 introduces Self Organizing Road Map Algorithm. Finally, in Section 2.6 Markov Random Fields (MRF) will be explained.

2.1 One Class Support Vector Machine (OCSVM)

The standard SVM is a classification technique introduced by Cortes and Vapnik (1995). The main idea of SVM is to map the input data into a high dimensional feature space corresponding to a kernel, and separate the classes with a linear decision function in this space. With the possibility of choosing different types of kernel, the linear decision functions in the mapped feature space are equivalent to a variety of non-linear decision functions in the input feature space.

The one-class SVM method developed by Schölkopf et al. (1999) is extended the SVM methodology for estimating the support of a high-dimensional distribution. Essentially, the strategy in this technique is the same as the standard SVM except that the decision function separates the data from the origin. Given a training data without any class information (2.2):

$$x_i \in R^n, i = 1,2, \dots, n \tag{2.1}$$

The primal form of one-class SVM is as follows

$$\min_{w,\rho,\xi}\left(\frac{1}{2}\boldsymbol{w}^T\boldsymbol{w} - \rho + \frac{1}{\nu n}\sum_{i=1}^{n}\xi_i\right) \tag{2.2}$$

$$\text{subject to} \quad \begin{cases} \boldsymbol{w}^T\Phi(x_i) \geq \rho - \xi_i, \\ \xi_i \geq 0, i = 1, \dots, n \end{cases}$$

where Φ is map function which is mapping the input space to a usually higher dimensional feature space where the data samples become linearly separable. SVMs introduce slack variables ξ_i to handle the case of points on the wrong side of the decision boundary.

The one-class SVM uses a parameter $\nu \in (0.1)$ to control the trade between training error and model complexity. We call this tradeoff strategy as ν-tradeoff.

The dual problem of one-class SVM is:

$$\min_{\boldsymbol{\alpha}} \frac{1}{2}\boldsymbol{\alpha^T Q \alpha} \tag{2.3}$$

$$\text{subject to} \quad \begin{cases} 0 \le \boldsymbol{\alpha_i} \le \dfrac{1}{\boldsymbol{vn}}, i = 1, \dots, n \\ \sum \boldsymbol{\alpha_i} = 1 \end{cases}$$

where $Q_{ij} = K(x_i, x_j) = \Phi(x_i)^T \Phi(x_j)$ is the kernel function. The solution $\boldsymbol{\alpha}$ of (2.4) is used to compute $\boldsymbol{w}$ and ρ in (2.3).

Some common kernel functions include linear, sigmoid, polynomial and Gaussian kernels. The Gaussian kernel, which is given by

$$\mathrm{k(x, y)} = \mathrm{e}^{-\frac{||\mathrm{x-y}||^2}{2}} \tag{2.4}$$

has been popular for practical use. The Gaussian kernel is employed due to its simplicity and efficiency.

2.2 Gaussian Mixture Model

GMM is a parametric probability density function expressed as weighted average of finite Gaussian component densities. It assumes the underlying data belong to a mixture of Gaussian distributions. It generally provides a better model than the single Gaussian densities for complex distributions. Each Gaussian , $i = 1,2, \dots, M,$ has its own mean $\boldsymbol{\mu}_i$ and covariance matrix $\boldsymbol{\Sigma}_i$ that has to be estimated separately.

$$g(\boldsymbol{x}|\boldsymbol{\mu_i}, \boldsymbol{\Sigma_i}) = \frac{1}{(2\pi)^{D/2}|\boldsymbol{\Sigma}_i|^{1/2}} \exp\left\{-\frac{1}{2}(\boldsymbol{x} - \boldsymbol{\mu}_i)^T \Sigma_i^{-1} (\boldsymbol{x} - \boldsymbol{\mu}_i)\right\} \tag{2.5}$$

The complete Gaussian mixture model can be expressed in terms of the mean vectors, covariance matrices and mixture weights corresponding to all mixture components. These parameters are represented by notation,

$$\lambda = \{w_i, \mu_i, \Sigma_i\} \quad i = 1, \dots, M. \tag{2.6}$$

In order to estimate the parameters of mixture distribution, λ, which best satisfy the distribution of the training data, a well-established method which is called maximum likelihood (ML) estimation is generally used.

The objective of ML estimation is to find the parameters of mixture model which maximize the likelihood of the GMM given the training vectors. Under the assumption of independence between the training vectors $X = \{x_1, \dots, x_T\}$, the GMM likelihood can be written as,

$$p(X|\lambda) = \prod_{t=1}^{T} p(\boldsymbol{x}_t|\lambda) \tag{2.7}$$

Since this expression is a non-linear function of the parameters λ and it is not possible to solve the problem analytically. However, parameter estimation can be achieved iteratively by using expectation-maximization (EM) algorithm.

GMM parameters (mean vectors, covariance matrices, and mixture coefficients) are estimated from training data using the iterative Expectation-Maximization Algorithm (EM).

EM is a maximum likelihood algorithm for fitting a mixture model to a set of training data. The basic idea of the EM algorithm is, starting with an initial model λ, to estimate a new model $\bar{\lambda}$, such that $p(X|\bar{\lambda}) \geq p(X|\lambda)$. Then new model becomes initial model for the next iteration and the process is repeated until some convergence threshold is reached.

On each EM iteration, the following re-estimation formulas are used which guarantee a monotonic increase in the model's likelihood value,

Mixture Weights

$$w_i^{(j+1)} = \frac{1}{T}\sum_{t=1}^{T} P_r(i|\boldsymbol{x_t}, \lambda^{(j)}) \tag{2.8}$$

Mean

$$\boldsymbol{\mu_i^{(j+1)}} = \frac{\sum_{t=1}^{T} \Pr(i|\boldsymbol{x_t}, \lambda^{(j)})\, x_t}{\sum_{t=1}^{T} \Pr(i|\boldsymbol{x_t}, \lambda^{(j)})} \tag{2.9}$$

Covariance Matrix

$$\boldsymbol{\Sigma_i^{(j+1)}} = \frac{\sum_{t=1}^{T} \Pr(i|\boldsymbol{x_t}, \lambda^{(j)}) \left(\boldsymbol{x_t} - \boldsymbol{\mu_i^{(j)}}\right)\left(\boldsymbol{x_t} - \boldsymbol{\mu_i^{(j)}}\right)^T}{\sum_{t=1}^{T} \Pr(i|\boldsymbol{x_t}, \lambda^{(j)})} \tag{2.10}$$

where $\boldsymbol{w_i^{(j)}}, \boldsymbol{\mu_i^{(j)}}, and\ \Sigma_i^{(j)}$ are the estimated parameters of i^{th} mixture component at j^{th} iteration. The a posteriori probability for components i is given by,

$$p(X|\lambda) = \frac{w_i g(\boldsymbol{x_t}|\boldsymbol{\mu_i}, \boldsymbol{\Sigma_i})}{\sum_{k=1}^{M} w_k g(\boldsymbol{x_t}|\boldsymbol{\mu_k}, \boldsymbol{\Sigma_k})} \tag{2.11}$$

A main drawback of GMMs is that the number of Gaussians mixture components is assumed to known as prior. Another problem arises with the correct initialization of the mixture components. A poor choice of initial parameters will invariably lead to poor results, as the EM algorithm converges only to a local optimization point.

2.3 Anti-parallel Centerline Extraction (ACE)

Several road network extraction approaches require road seed points before algorithm can continue with extraction process. These seed points are generally specified by a human operator. Automating the seed point extraction process eliminates human intervention and thus reduces the extraction time. In the existing literature, several techniques are proposed to detect road seed points automatically. These methods are generally based on parallel edge detection, road structure matching, segmentation, etc.

Anti-parallel Centerline Extraction (ACE) proposed by Doucette et al. (2004) presents a more advanced approach for the seed point extraction. The algorithm is based on the detecting parallel edges. Since roads are shown as either brighter or darker than the background, among detected parallel edges only the ones with opposing gradients are selected as candidate seed points. These edges are often referred as Anti-Parallel (APAR) edges. Besides gradient criterion, there are also minimum and maximum distance thresholds which are controlling the acceptable range of road widths. After the parallel edges satisfying these criteria are detected, the candidate road centerline points are placed hallway between the edges.

The intensity and gradient profiles of a road cross-section are shown in Figure 2-1. The road edges are visible as two local extrema with opposing signs in the gradient plot (Figure 2-1.c). The ACE algorithm is designed to search for these patterns and locate a road centerline points between these two extrema.

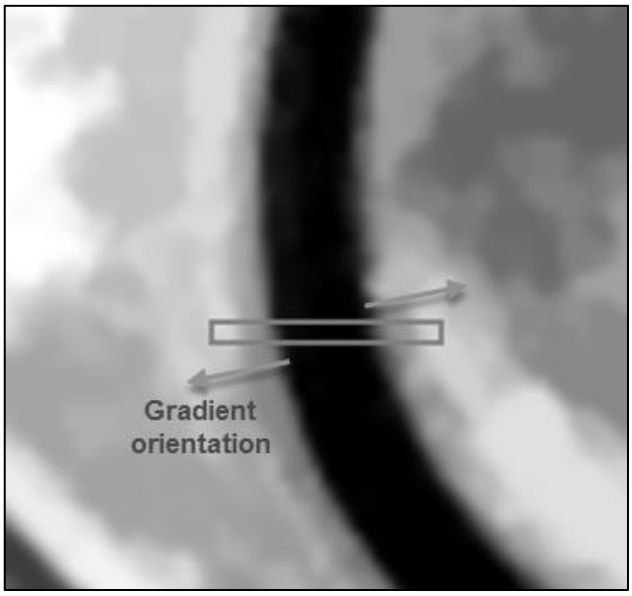

(a)

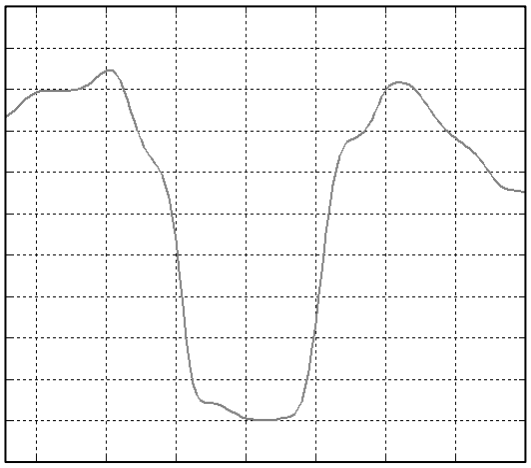

(b)

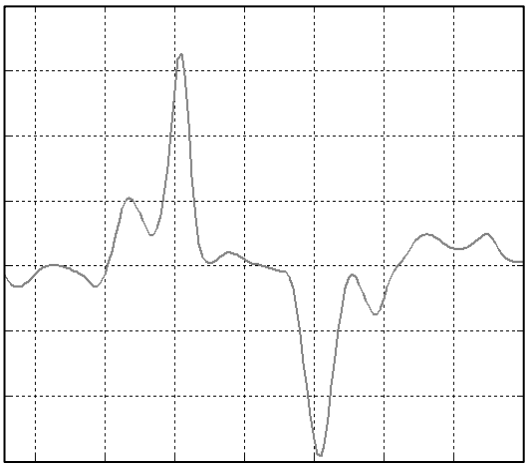

(c)

Figure 2-1 Gradient signature for roads: (a) Input image, (b) Image intensity profile, (c) gradient intensity profile.

The ACE algorithm can be summarized as follows: First, an edge detector is used to locate edges within the image. Then, gradient directions are determined by convolving the image with 3x3 Sobel operators, S_x and S_y. After horizontal and vertical gradients are determined (Eq. 2.13), gradient direction is calculated by the formula in Eq. (2.14).

$$Horizontal\ Sobel\ operator: S_x = \begin{bmatrix} -1 & 0 & +1 \\ -2 & 0 & +2 \\ -1 & 0 & +1 \end{bmatrix}$$

$$Vertical\ Sobel\ operator: \quad S_y = \begin{bmatrix} -1 & -2 & -1 \\ 0 & 0 & 0 \\ -1 & +2 & +1 \end{bmatrix}$$

$$Horizontal\ gradient: G_x = S_x * Image$$
$$Vertical\ gradient: \quad G_y = S_x * Image \tag{2.12}$$

$$Gradient\ direction: \varphi = \tan^{-1}(\frac{G_y}{G_x}) \tag{2.13}$$

Then, the edge image is scanned in both horizontal and vertical directions to obtain the pixels satisfying the distance and gradient orientation conditions. Figure 2-2 illustrates an ACE horizontal scan line that first finds an edge pixel *p*, and next finds an edge pixel *q* on the same row. If the angle between gradient orientations, Φ_p and Φ_q at pixels p and q is approximately 180^o and the distance between pixels p and q are within a certain road width range, a centerline pixel m is tagged at the midpoint between *p* and *q*.

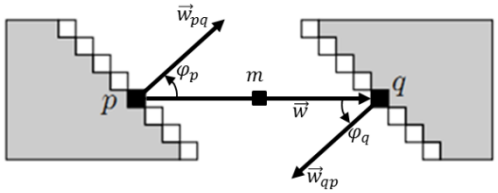

Figure 2-2 ACE horizontal scan line.

Figure 2-3.b presents the Canny edges of the sample scene displayed in Figure 2-3.a. Figure 2-3.c illustrates the APAR edges obtained by horizontal scan of Canny edges, while Figure 2-3.d depicts the APAR edges obtained by vertical scan. The final output by ACE algorithm is illustrated in Figure 2-3.e which is the horizontal and vertical APAR edges combined. As the result is noisy, a connected components analysis is performed to remove small connected pixels (Figure 2-3.f).

(a) Original Image

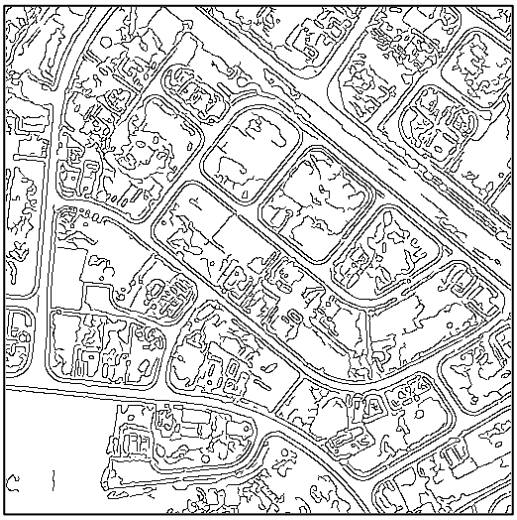

(b) Canny Edges

(c) Horizontal APAR Edges

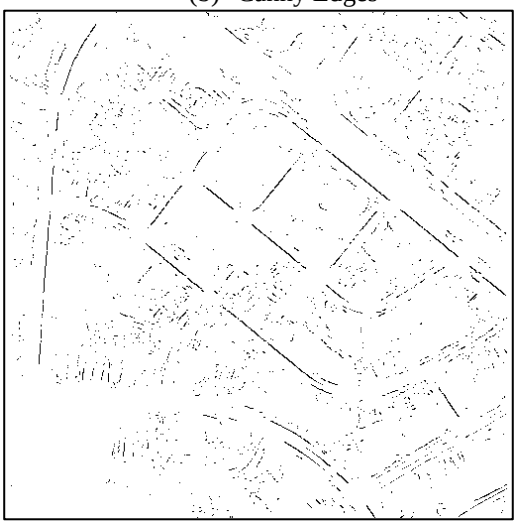

(d) Vertical APAR Edges

(e) All APAR Edges

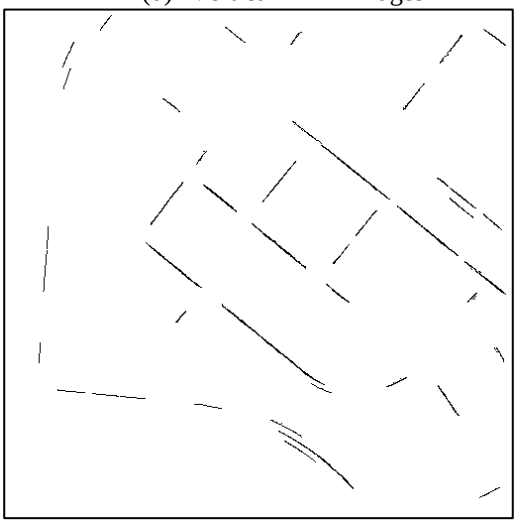

(f) APAR Edges (small connected components removed)

Figure 2-3 ACE Algorithm steps

2.4 Principal Component Analysis

Multispectral image bands are often highly correlated, i.e., they are visually and numerically similar. The scatter diagrams of neighboring spectral bands for a test image (Figure 2-4.a) are presented in Figure 2-4. Correlation coefficients of these spectral bands are listed in Table 2-1. As can be seen from this table, the correlations between bands are very high. Because of this spectral redundancy, analysis of all spectral bands is inefficient. Principal Component Analysis (PCA) is a statistical technique designed to remove this spectral redundancy.

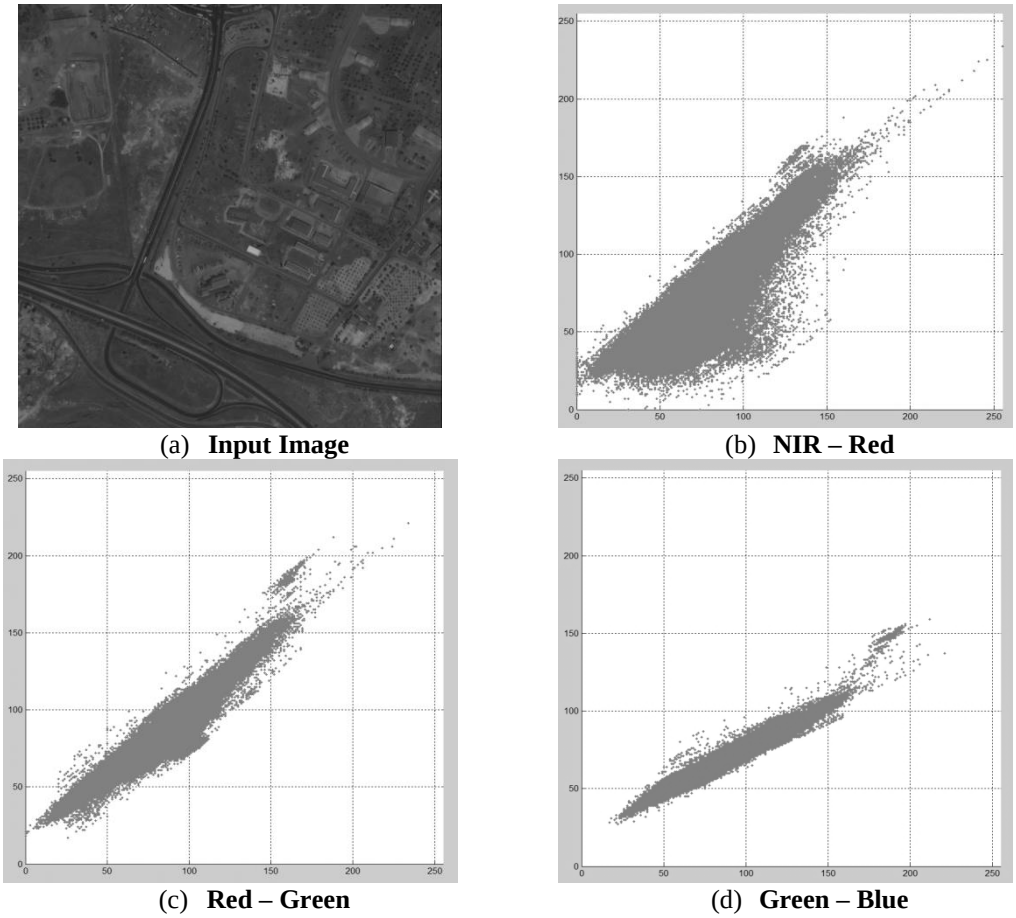

Figure 2-4 Scatter diagram (SD) of spectral bands: (a) Input Image; (b) SD of NIR versus R ; (c) SD of Red versus Green; (d) SD of Green versus Blue bands.

Table 2-1 Correlation Coefficients of Spectral Bands of a sample satellite image.

Correlation	Near Infrared	Red	Green	Blue
Near Infrared	1.00	0.89	0.83	0.69
Red	0.89	1.00	0.96	0.88
Green	0.83	0.96	1.00	0.97
Blue	0.69	0.88	0.97	1.00

CA is a feature transformation to reduce a set of correlated features to a smaller set where features are uncorrelated and retain most of the original information (Ready & Wintz, 1973). It is a linear transformation of the image data matrix $\boldsymbol{X}$ (m samples, n features), with an image specific transformation matrix $\boldsymbol{W}$ (m x m),

$$\boldsymbol{X_{PC}} = \boldsymbol{WX} \tag{2.14}$$

The transformed covariance matrix $\boldsymbol{\Sigma}_{PC}$ is calculated as follows:

$$\boldsymbol{\Sigma_{PC}} = \boldsymbol{E}\{\boldsymbol{X_{PC}X_{PC}^T}\} = \boldsymbol{E}\{\boldsymbol{WXX^TW^T}\} = \boldsymbol{WE}\{\boldsymbol{XX^T}\}\boldsymbol{W^T} = \boldsymbol{W\Sigma W^T} \tag{2.15}$$

where $\boldsymbol{\Sigma}$ is the covariance matrix of original data. The PCA finds the transformation $\boldsymbol{W}$ that diagonalizes the covariance matrix of the original multispectral image, so that,

$$\boldsymbol{\Sigma_{PC}} = \begin{bmatrix} \lambda_1 & \dots & 0 \\ \dots & & \dots \\ 0 & \dots & \lambda_K \end{bmatrix} \tag{2.16}$$

The eigenvalues of $\boldsymbol{\Sigma}$ can be calculated from its characteristic equation:

$$|\boldsymbol{\Sigma} - \boldsymbol{\lambda I}| = 0 \tag{2.17}$$

where **I** is an m-dimensional identity matrix.

The four Principal Components (PC) images of the image in Figure 2-4.a are shown in Figure 2-5. These features are statistically uncorrelated. The scatter diagram of PC1 and PC2 is shown in Figure 2-6.

As can be seen from Table 2-2, the total variance captured by PC1 and PC2 is about 98%. This also means that most of the information captured by these two components. Therefore, only PC1 and PC2 can be used in image analysis instead of original multi-spectral images.

Table 2-2 Principal Component Analysis

PC Number	Eigenvalue of Correlation Matrix	% Variance Captured	% Variance Captured Total
1	3.62	90.48	90.48
2	0.33	8.20	98.68
3	0.047	1.16	99.85
4	0.0062	0.15	100.00

(a) PC1 Image

(b) PC2 Image

(c) PC3 Image

(d) PC4 Image

Figure 2-5 Principal Component Images

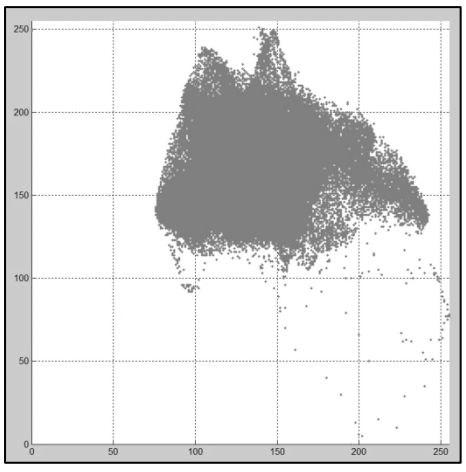

Figure 2-6 Scatter Diagram of PC1 and PC2

2.5 Self-Organizing Road Map

Doucette et al. (2001) proposed a self-organizing road map (SORM) to delineate road centerlines from classified high-resolution Multi-Spectral Imagery (MSI). SORM algorithm inspired from the neural network model called Self-Organizing Map (SOM) (2001).The SORM is basically a spatial clustering algorithm which is adapted to find and link elongated image regions.

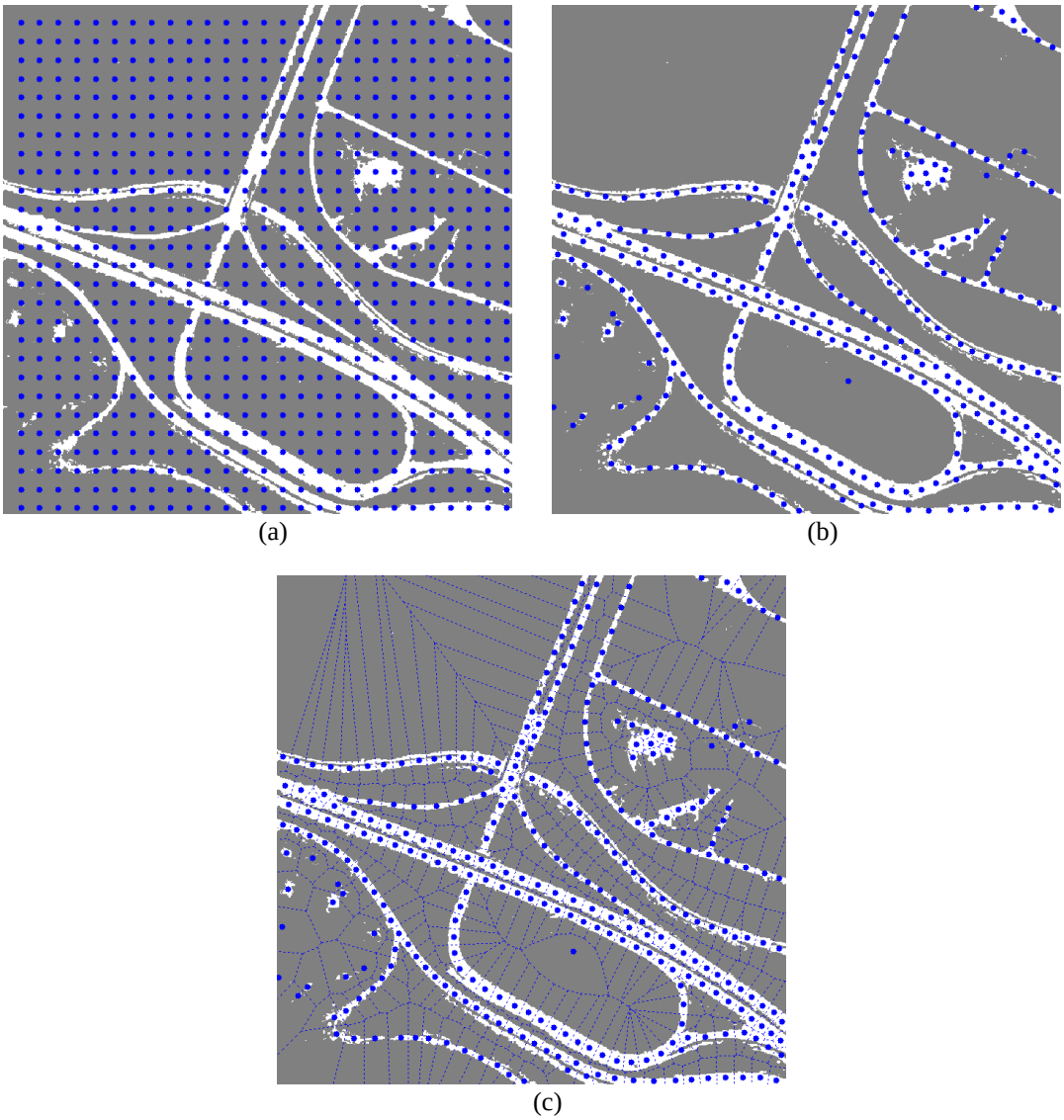

(a) (b)

(c)

Figure 2-7 The SORM process: (a) Initial cluster centroids, (b) K-medians Clustering, (c) Voronoi regions for each cluster center.

The SORM approach integrates a K-medians clustering algorithm with a node linking minimum spanning tree (MST) algorithm. The process begins with a classified binary image as input to K-medians algorithm. K-medians algorithm is similar to well-known clustering algorithm K-means. However, in this case, a median computation is substituted for the mean calculation. The purpose of using median statistics instead of mean is to reduce the effect of outliers because the median statistics is more robust estimator than the mean. An evenly spaced grid is created across the image, where every grid point on the image represents a cluster centroid (Figure 2-7.a). Grid spacing is determined by considering the maximum road width and minimum road length. After initialization of cluster centroids, SORM updates each centroid locations by computing the medians of road pixel locations within the Voronoi cell of cluster centroid. The locations of cluster centroids are updated iteratively until no further changes occur. At the end, clusters with unchanged centroids are marked as dead and removed (Figure 2-7.b). The remaining active cluster centroids are illustrated in the Voronoi diagram in Figure 2-7.c.

In the second stage of the algorithm, a MST based linking algorithm is used to derive a consistent topology from the convergent cluster locations. Refer to original paper for detailed description of this stage. In this work, K-median algorithm is used to detect candidate road centerline points. These points are connected with a MRF based network topology extraction approach instead of the MST proposed in the original SORM algorithm.

2.6 Markov Random Fields

Markov Random Field provides a way of modeling contextually dependent objects such as image pixels, regions and edge components. MRF has been used for solving vision problems at various processing levels from low-to-high. These problems include image restoration, image completion, segmentation, texture synthesis, super-resolution, stereo matching, object matching and recognition.

Markov Random Field is a graphical model for n-dimensional random process defined on a set of sites S. These sites may be regularly spaced on a lattice (Figure 2-8.a) or irregularly spaced (Figure 2-8.b). In an MRF, a site $s \in S$ is related to one another via a neighborhood system, which is defined as:

$\mathcal{N} = \{\mathcal{N}_i | \forall i \, \epsilon S\}$, where $\mathcal{N}_i$ is the set of sites neighboring i, such that $i \notin \mathcal{N}_i$, $i \in \mathcal{N}_j \Leftrightarrow j \in \mathcal{N}_i$.

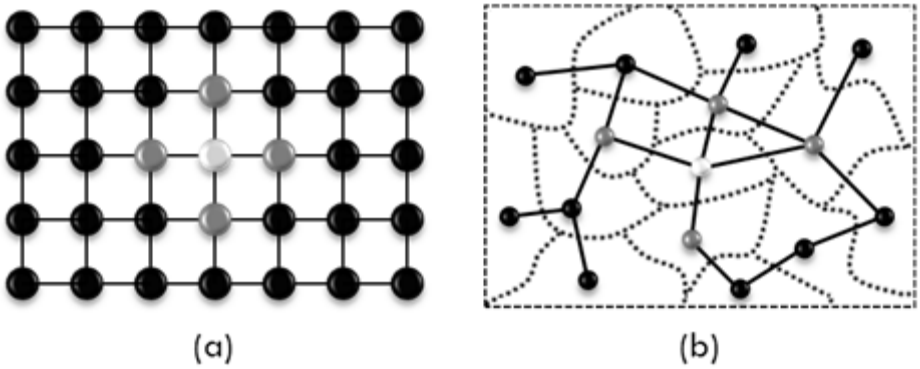

Figure 2-8 (a) Regularly spaced sites, (b) Irregularly spaced sites.

A Markov Network consists of an undirected graph $G = (V, E)$, where each node $v \in V$ represents a random variable and each edge $\{u, v\} \in E$ capture the statistical dependency between random variables. This set of random variables form a Markov Random Field on S with respect to neighborhood system $\mathcal{N}$ if they satisfy the Local Markov property:

Pair-wise Markov Property: Any two non-adjacent variables are conditionally independent given all other variables:

$$p(x_i, x_j | \boldsymbol{x}_{V\setminus\{i,j\}}) = p(x_i | \boldsymbol{x}_{V\setminus\{i,j\}}) p(x_j | \boldsymbol{x}_{V\setminus\{i,j\}}) \quad (2.18)$$

Local Markov Property: A variable is conditionally independent from the rest of variables given its neighbors:

$$p(x_i | x_{V\setminus\{i\}}) = p(x_i | x_{N(i)}) \quad (2.19)$$

where $N(i)$ is the set of neighbors of i.

Global Markov Property: Any subsets of variables are conditionally independent given a separating subset:

$$p(x_A, x_B | x_S) = p(x_A | x_S) p(x_B | x_S), \quad (2.20)$$

where every path from a node in A to a node in B passes through S.

Since the joint probability distribution of a random process with arbitrary distribution is possibly difficult to establish, the practical use of MRF models is commonly described by a theorem established by Hammersley & Clifford (1971) and further improved by Besag (1974). The theorem is stating that the joint distribution of an MRF is a Gibbs distribution. A Gibbs distribution is defined as

$$P(X) = \frac{1}{Z} e^{\frac{U(X)}{T}} \quad (2.21)$$

where Z is a normalizing constant called the partition function, T is a constant called temperature and U is the energy function. The energy $U(x) = \sum_{c \in C} V_c(X)$ is a sum of clique potentials V_c over all possible cliques $c \in C$.

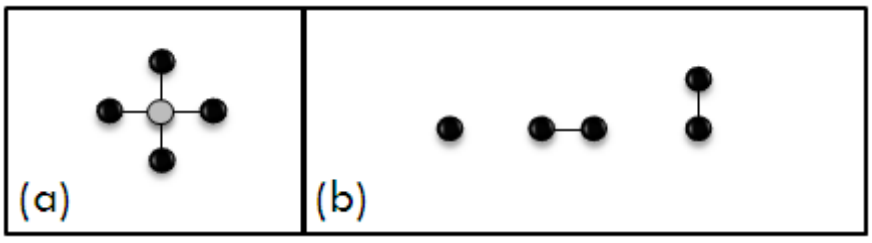

Figure 2-9 (a) Four-neighborhood system, (b) clique types

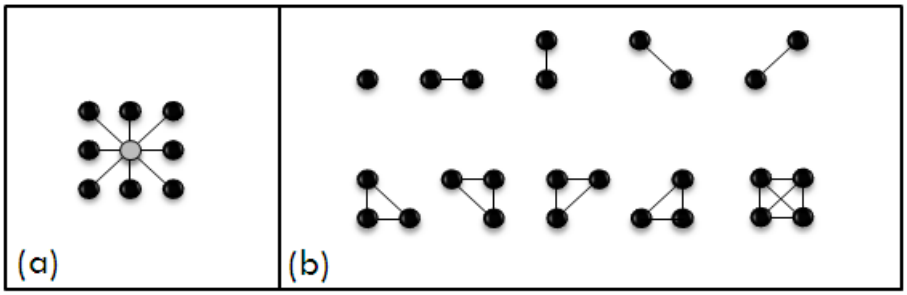

Figure 2-10 (a) Eight-neighborhood system, (b) clique types

A clique is a subset of nodes in which every node is connected to every other node. A maximal clique is a clique which cannot be extended by the addition of another node. Figure 2-10 shows clique types for a regular lattice. Cliques for irregularly placed sites do not have well defined shapes as those for a regular lattice. Therefore, their types depend on how the neighborhood relations defined between sites. A simple way is to connect two nodes if the distance between them is less than a pre-defined threshold. Figure 2-11 shows clique types for an irregular lattice.

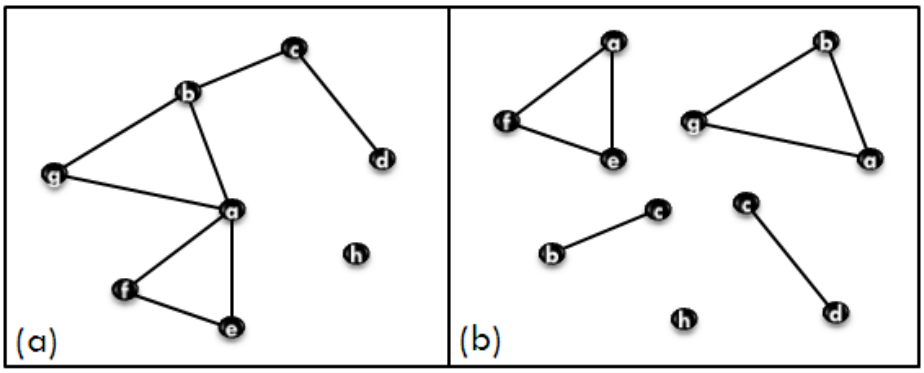

Figure 2-11 (a) Irregular sites and (b) maximal clique set

Consider a random field X on a graph G, such that $p(X) > 0$. Let C denote the set of all maximal cliques of the graph. If the field has the local Markov property, then $p(X)$ can be written as a Gibbs distribution:

$$p(x) = \frac{1}{Z}\exp\left\{-\sum_{c\in C} V_c(\boldsymbol{x}_c)\right\} \tag{2.22}$$

where Z, the normalizing constant, is called the partition function; $V_c(x_c)$ are the clique potentials.

If $p(x)$ can be written as a Gibbs distribution for the cliques of some graph, then it has the global Markov property. As a result, a Markov Random Field (MRF) can be expressed in terms of its clique potentials.

CHAPTER 3

PROPOSED ROAD NETWORK EXTRACTION ALGORITHM

In this chapter, the proposed road network extraction framework will be explained. The framework is composed of different methods integrated into a complete road network extraction system.

This chapter presents a description of the framework in Section 3.1, followed by sections providing detailed information on each stage of the framework. Section 3.2 describes the Spectral Classification techniques. The road class refinement methodologies are discussed in Section 3.3, while Section 0 discusses the centerline extraction methods. The MRF based road network formation approach is provided in Section 3.5. The chapter is concluded in Section 3.6.

3.1 Proposed Algorithm

A flowchart of proposed road network extraction algorithm is given in Figure 3-1. A four-staged algorithm is proposed to detect road network from high resolution multi-spectral images (MSI). The algorithm starts with a Spectral Classification which converts multi-spectral image into a binary or grey-level image. The output image of classification gives the probability of a pixel belonging to a road class and it is called "*potential image*". After the classification of image, Road Class Refinement step is employed to increase the classification accuracy. The refined potential image are then clustered with K-Medians clustering algorithm in the Road Centerline Extraction Step. In the final stage, the extracted cluster centroids are used to construct road network. In the following sections, detailed information on methodologies used in each stage will be provided.

3.2 Spectral Classification

The objective of spectral classification is to separate roads from non-road regions using spectral information of Multi-spectral Images (MSI). After classification is performed, the image is classified into two groups of categories: a road group and a non-road group.

Figure 3-2 illustrates an example of the output created by a spectral classifier, where brighter values indicate a higher probability of a pixel belonging to the road class. As we can see in this figure, the major issue with spectral classification is the misclassification between roads and other spectrally similar objects, such as open parking lots, shadows, building, etc.

Classification method starts with a pre-filtering stage to smooth the image. Then the features to be used during classification are determined in feature selection stage followed by a training set selection stage to extract training data. The classification progresses with a training stage where a road model will be generated based on the selected training data. Then classification concludes by producing road potential image which is corresponding to probability of a pixel belonging to road class.

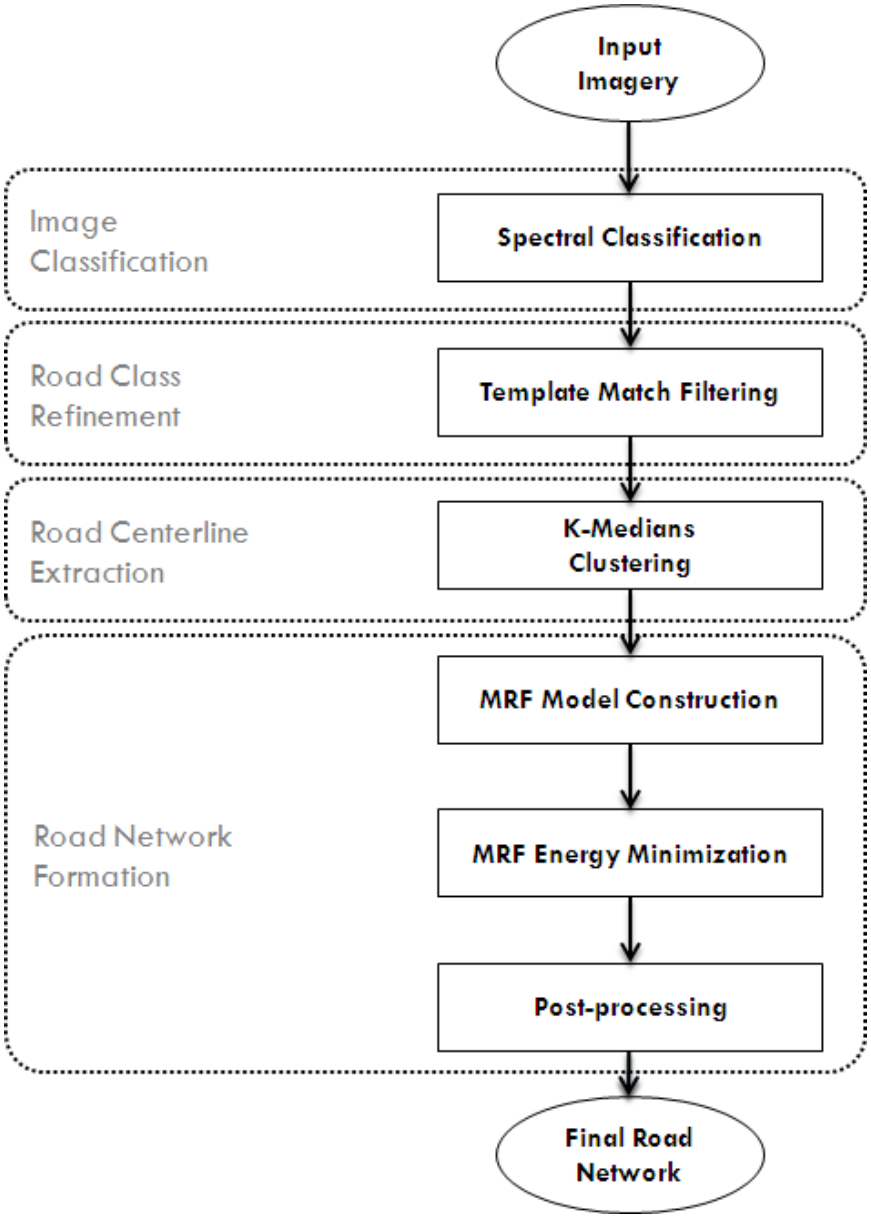

Figure 3-1 Flowchart of Road Network Extraction system

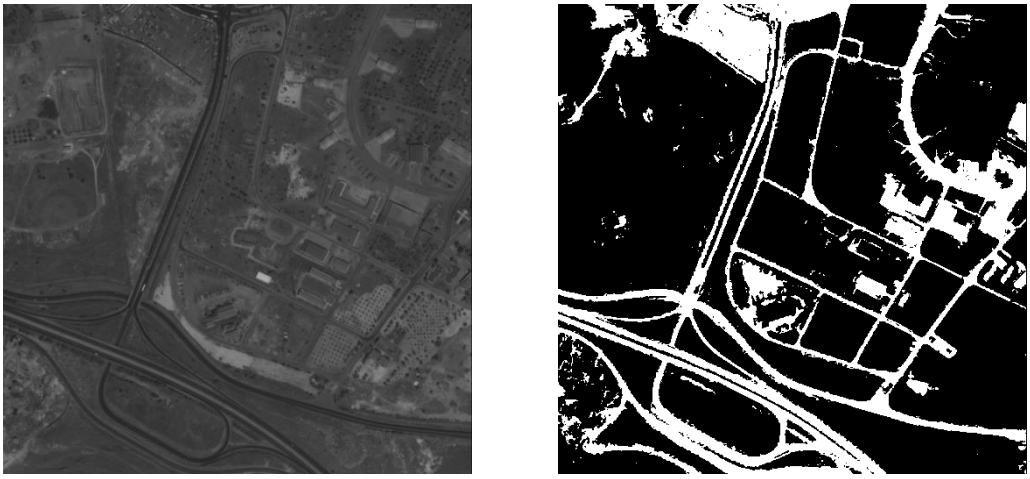

(a) (b)

Figure 3-2 An example of spectrally classified image: (a) Original image, (b) Road potential image.

3.2.1 Feature Selection

Although original spectral features are useful for visual representation, they may not be very convenient for spectral classification. As stated in section 0, the original spectral features are highly correlated. Therefore, the principal components obtained by PCA (see section 0) as an alternative feature set that may provide a better feature representation than the original spectral features.

The variance captured by each principal component for a set of Multi-spectral (R, G, B, NIR) test images are listed in Table 3-1 . These results show that the total variance captured by only PC1 and PC2 is more than 98% for all images. This means that the multi-spectral images can be represented by PC1 and PC2 without losing any significant information. Using principal components instead of original spectral features is computationally more economical because it contains less number of features.

Table 3-1 PCA results of Multi-spectral test images (1-m spatial resolution, 512 by 512 pixels)

	% Variance Captured by			
Image No	**PC1**	**PC2**	**PC3**	**PC4**
1	80.99	17.82	0.99	0.21
2	85.51	13.41	0.85	0.23
3	84.63	13.95	1.22	0.21
4	84.72	14.39	0.62	0.27
5	87.26	11.85	0.72	0.17
6	81.86	17.10	0.90	0.14
7	86.01	12.90	0.84	0.24
8	83.39	15.76	0.65	0.19
9	81.66	17.02	1.09	0.22
10	75.91	22.60	1.29	0.19
11	74.49	23.99	1.38	0.13
12	82.56	16.56	0.72	0.16

3.2.2 Training Set Selection

In manual (or automatic) training set selection, only road class samples are provided and there is no information available about the distribution of non-road class. Therefore, in this work, only one-class classification is used to distinguish road class pixels. Our aim is to find a decision function that best models the distribution of the spectral feature of pixels belonging to road class.

The training set regions can be provided by a human operator. This process can also be automatized with an automatic seed extraction algorithm. In this study, Anti-Parallel Centerline Extraction algorithm (ACE) is used to detect road seed points.

As mentioned in the previous section, ACE is based on the assumption that roads are elongated-shape and have opposite gradients on the different sides. All the regions that are satisfy these assumptions are extracted as road centerline. This could cause some regions falsely detected as roads like the regions between parallel roads.

If the amount of false detected samples in the training set increase, the classification performance degrades significantly. The succeeding road network extraction algorithms are based on the assumption that the classification accuracy is moderately high. Otherwise, the algorithm will fail to extract road network properly. Therefore, in order to evaluate the performance of the algorithms properly, the results obtained via manually extracted training data are used first. Then, the performance of automatic training is evaluated separately.

Although, Training set selection can be automatized by this way, still need an operator to control detected regions.

3.2.3 Training a Classifier

Roads have similar spectral signature. However the spectral properties of non-road regions are not known. If the training data which belongs to non-road class is not chosen properly, this can lead to problem of over-fitting. Therefore, in this thesis, one-class classification (i.e. distribution estimation) methodologies are used.

Two different classification methods is used, Gaussian Mixture Models (GMM) and Support Vector Machines (SVM). Since only the samples from road class are available, One-class SVM is used instead of standard SVM methodology. In the following sections, the performance of these classifiers is analyzed.

3.2.3.1 Modeling with One Class SVM

One-class SVM introduced by Schölkopf et al. (1999) for estimating the support of a high-dimensional distribution. As it is discussed in Section 2.1, the one-class SVM constructs a decision function that takes the value +1 in a small region capturing most of the training data, and –1 elsewhere.

The OC-SVM introduces a parameter (rejection rate) $v \in (0,1)$ to control the percentage of outliers in training data. It is shown in Schölkopf et al. (1999) that the parameter v is an upper bound on the fraction of outliers (FO), i.e. training data points outside the decision region of one-class SVM, and it is a lower bound on the fraction of support vectors (FSV) in the training data.

The effect of the parameter v can be observed through the following classification results. The distribution of training data for features PC1 and PC2 is illustrated as a scatter diagram in Figure 3-3. Decision boundaries obtained by OC-SVM algorithm are also shown. Results are generated for four values of v: 0.01, 0.04, 0.07 and 0.1 while keeping other parameters constant. As we can see, the size of decision boundary decreases while increasing v. The training data outside the decision boundary, on the other hand, increases.

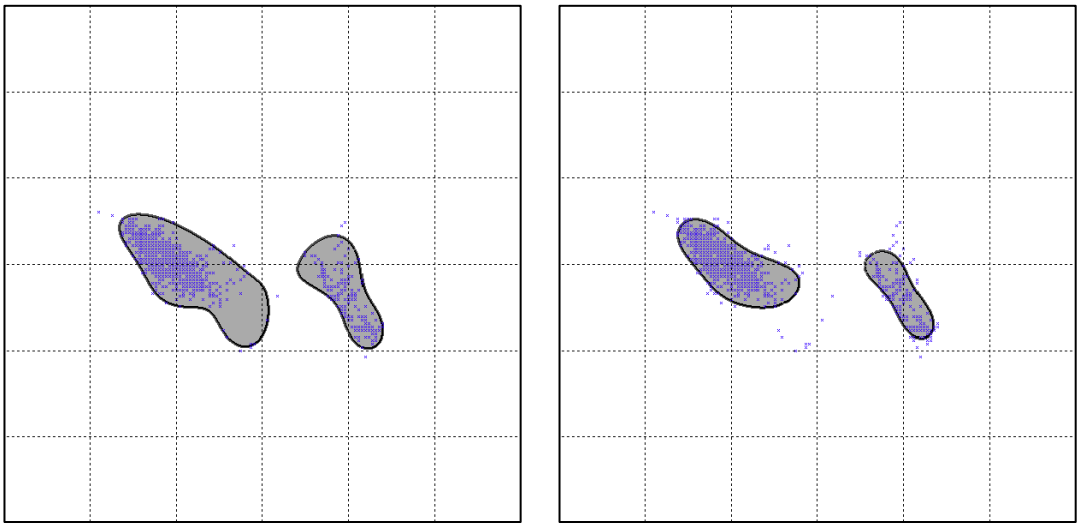

(a) $v = 0.01$ (b) $v = 0.04$

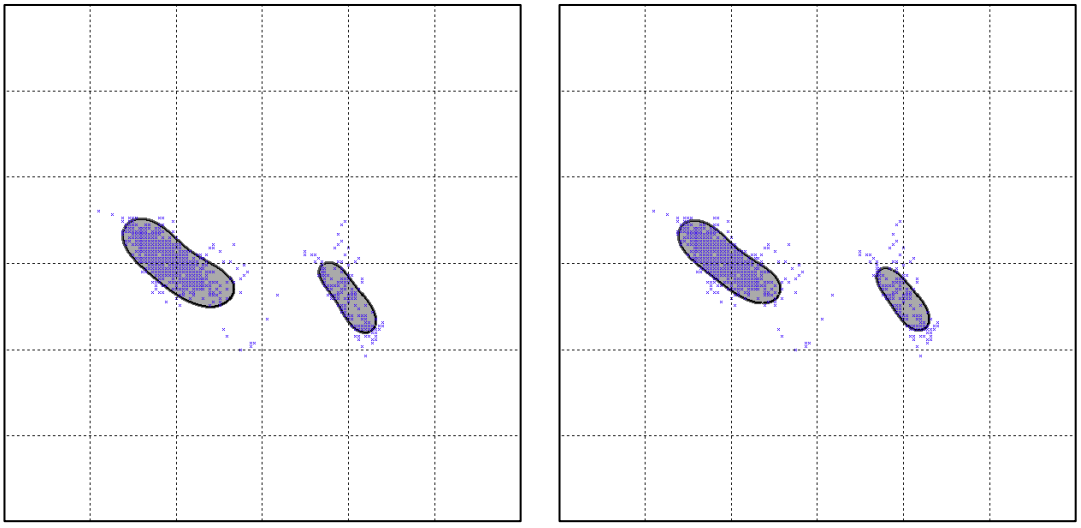

(c) $v = 0.07$ (d) $v = 0.10$

Figure 3-3 OC-SVM Decision Boundary for features PC1 and PC2

There is another parameter, σ, in case Gaussian kernel is used. Tuning this parameter is performed with a technique called Cross-Validation (CV). CV is a popular strategy for optimum parameter selection. The main idea behind CV is to divide the training data into K groups of samples for evaluating the performance of each classification: Part of data is used for training the algorithm, and the remaining part is used for validation, that is for estimating the performance of the classification.

In order to estimate accuracy of classification algorithm, we do a search on parameter σ. For each value of σ, we employed a 10-fold cross-validation and evaluated the accuracy. Since there is no class labels in the one-class SVM, it is not possible to find optimum kernel parameters just by maximizing the CV accuracy, as it is common for a two-class SVM.

Therefore, a performance evaluation technique needs to be proposed based on following criteria.

1) Number of SVs should be minimized: Because It represents how complex is the decision boundary. When it starts to become complex, it loses its generalization ability by overlearning the training data. So it is important to keep the decision boundary simple as possible.
2) Size of decision region should be small. Because decision boundary should only contain the training data. However if the number of features are high, it is hard to compute size of decision region.

As a result, our aim is to find a minimum decision region which captures the most of the data while keeping the number of support vectors minimum and cross-validation accuracy maximum.

The size of decision region is computed by sampling the whole feature space with an appropriate sampling distance. The ratio of samples outside the decision region over all samples will give an idea about how large is the decision boundary. This parameter is called fraction of decision space (FDS). In case, PC1 and PC2 are used as feature set for classification, FDS can be computed without much computational load. However, if the number of features increases the computational cost of evaluating FDS will be huge.

The values of performance metrics CVA, FSV, FO and FDS while increasing v and s-parameters are provided in Table 3-2. As it is stated before both FSV and FDS should be minimized. On the other hand, CVA needs to be maximized. Decreasing value of FDS can be achieved by increasing s-parameter. However in this case, the value of FSV will increase which is not desired. Therefore, we should determine a certain stopping criterion for s-parameter. In Figure 3-4, Cross Validation accuracy (CVA) values of OC-SVM algorithm for different value of s-parameter are plotted. As we can see, at some point, CVA begins to decrease quickly. The value of s-parameter, just before the sharp fall, will be used as optimum parameter.

The decision of v-parameter highly depends on how many outliers are contained in training data. For manually selected clean data sets, the value of v should be chosen small. On the other hand, for noisy training data, it should be chosen greater to compensate the noise. Our experimental results show that any value of v between 0.01 and 0.05 give satisfactory performance for our test images. Therefore, this value is set to 0.03 for the simplicity.

Table 3-2 OC-SVM parameter tuning

OC-SVM Parameters		**Cross Validation Accuracy (CVA) (%)**	**Fraction of Support Vectors (FSV) (%)**	**Fraction of Outliers (FO) (%)**	**Fraction of Decision Space (FDS) (%)**
ν	σ				
0.01	**0.5**	**99.0**	**1.0**	**1.0**	**7.4**
	1	99.0	1.0	1.0	7.0
	2	**99.0**	**1.0**	**1.0**	**6.1**
	4	99.0	1.0	1.0	4.5
	8	**99.0**	**1.0**	**1.0**	**3.7**
	16	99.0	1.0	1.0	3.1
	32	**98.9**	**1.1**	**1.0**	**2.4**
	64	98.5	1.2	1.5	2.0
	128	**96.6**	**1.6**	**2.8**	**1.9**
	256	91.6	3.2	8.0	1.6
	512	**85.1**	**4.9**	**15.5**	**1.4**
	1024	71.6	6.4	24.4	1.2
0.05	**0.5**	**94.9**	**1.0**	**5.0**	**6.6**
	1	95.3	1.0	5.0	6.2
	2	**94.9**	**1.0**	**5.0**	**5.5**
	4	95.1	1.0	5.0	4.1
	8	**95.0**	**1.0**	**5.0**	**2.6**
	16	94.9	1.0	5.0	2.2
	32	**94.9**	**1.1**	**5.1**	**1.4**
	64	94.3	1.2	5.1	1.1
	128	**94.4**	**1.6**	**5.3**	**1.1**
	256	93.1	3.2	5.8	1.0
	512	**90.6**	**4.9**	**7.8**	**1.0**
	1024	81.3	6.4	10.4	0.9
0.10	**0.5**	**90.2**	**1.0**	**10.0**	**5.2**
	1	90.2	1.0	10.0	5.0
	2	**90.1**	**1.0**	**10.0**	**4.5**
	4	90.3	1.0	10.0	3.5
	8	**89.8**	**1.0**	**10.0**	**2.2**
	16	89.7	1.0	10.0	1.6
	32	**89.8**	**1.1**	**10.1**	**1.0**
	64	90.2	1.2	10.1	0.8
	128	**89.6**	**1.6**	**10.2**	**0.8**
	256	88.6	3.2	10.6	0.7
	512	**87.4**	**4.9**	**11.6**	**0.7**
	1024	83.2	6.4	14.0	0.6

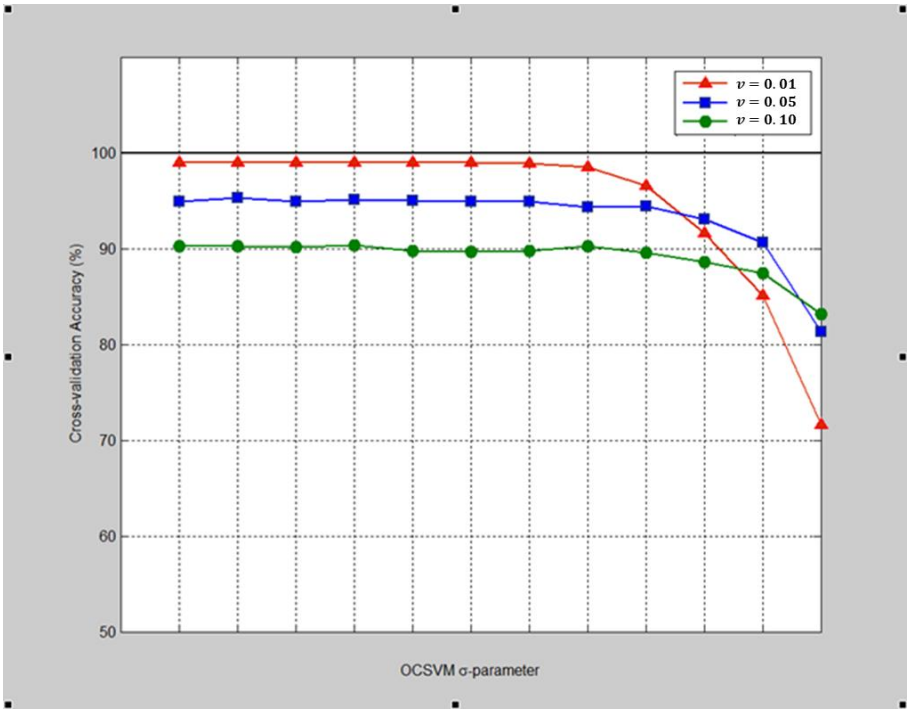

Figure 3-4 Cross-validation Accuracy change w.r.t. $\boldsymbol{\sigma}$-parameter for $\boldsymbol{v}$ = 0.01, 0.05, 0.10

3.2.3.2 Modeling with Gaussian Mixture Model

Road model based on a single Gaussian may not be enough, if the distribution of road class is complex. Therefore, it will be more convenient to use a mixture of Gaussian model. A main drawback of GMMs is that the number of Gaussians mixture components is assumed to known as prior. The optimum number can be found with a technique similar to one used in OC-SVM section. However in this case, our aim is to find an optimum number of Gaussian Components that will model both road class and outliers in the training data set.

Optimality of mixture model is defined based on these three criteria:

1. Number of Gaussians should be minimized so that model should be simple.
2. Most of the training data should be captured by the model.
3. The space within the decision boundary should be minimized.

Algorithm starts with a mixture model which has $N = 2$ components and N is increased by one at each iteration up to a predefined parameter N_{max} showing maximum number of components. At each iteration, all combination of K, $K = 1, 2, \dots, N-1$, Gaussian components that captures at least a specified threshold of the minimum capture percentage C_{min} taken as a possible solution. Among these solutions, the one which best satisfy the three criteria is taken as the optimum mixture model.

The total number of mixture combinations at each iteration is $(N-1)!$. If N is too large, there will be a lot of solutions need to be analyzed to determine whether it is optimal or not. Therefore N_{max} should be kept small.

The parameter C_{min} highly depends on the quality of training set. If the input image is noisy then it means there is a significant percentage of training data composed of outliers. Therefore, choosing C_{min} very high may reduce the classification accuracy due to the outliers in the training set. Empirical results show that, 85%-90% is good range for C_{min}.

There is another parameter need to be considered which is called fraction of decision space FDS. It is the ratio of the space under the decision boundary over whole feature space. FDS should be small as possible so that a tight model will be generated.

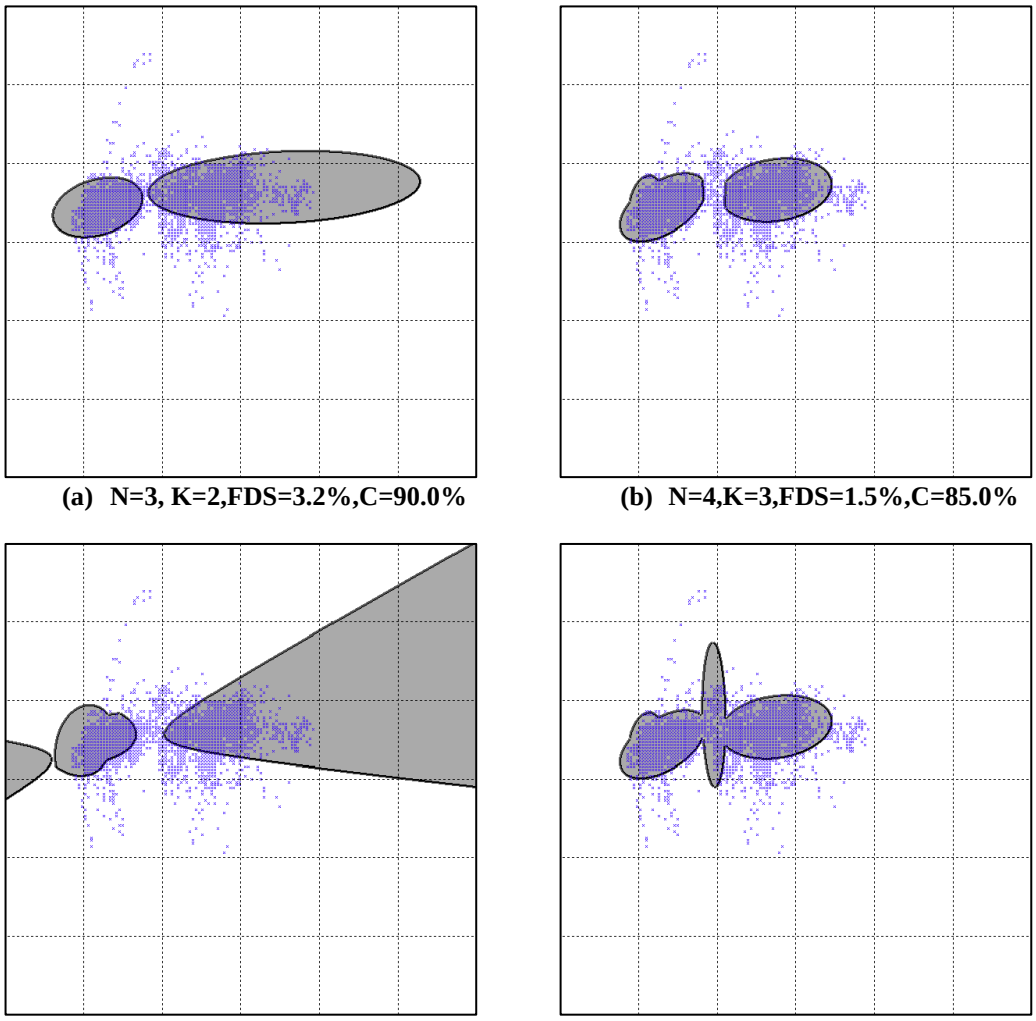

(a) N=3, K=2,FDS=3.2%,C=90.0% **(b) N=4,K=3,FDS=1.5%,C=85.0%**

(c) **N=5, K=3,FDS=18.4%,C=85.3%** **(d) N=5,K=4,FDS=2.0%, C=90.8%**

Figure 3-5 GMM candidate solutions

(a) Ground Truth

(b) N=3, K=2, FDS=3.2%, C=90.0%

(c) N=4, K=3, FDS=1.5%, C=85.0%

(d) N=5, K=4, FDS=18.4%, C=85.3%

(e) N=3, K=3,FDS=2.0%, 90.8%

Figure 3-6 Output of GMM classification

The acceptable solutions obtained with GMM for a test image are illustrated in Figure 3-5. The solution shown in Figure 3-5.c can be easily eliminated by comparing with the solution in Figure 3-5.d because the latter captures more training data (C) with still a small decision space (FDS). By eliminating poor results, the solution set can be reduced. Among the remaining set, the solution in Figure 3-5.d has given best performance because it has captured more training data with moderately small decision space. The result can be visually perceived from their associated classification results which are shown in Figure 3-6. Although, all of them have succeeded to completely extract roads, the one in Figure 3-5.d contains less number of false positives, i.e. pixels not belonging to road but identified as if belonging.

3.2.4 Evaluation of Classification Results

In this section, a performance comparison of two classification method, OC-SVM and GMM, is provided. In order to evaluate performance of classification algorithms quantitatively, there are some quality measures that have been used: the precision to indicate the ability of classification algorithms to extract all roads; recall to represent the percentage of correctly classified road pixels with respect to the total extracted road pixels; and the accuracy to indicate the ability of algorithms to classify image correctly. These quality metrics of extracted roads is calculated in terms of comparison elements: true positive (TP), true negative (TN), false positive (FP) and false negative (FN). These elements are explained as follows:

True Positive (TP): The extracted road pixels are consistent with the ground truth.

True Negative (TN): The areas where no roads are extracted are consistent with the ground truth.

False Positive (FP): The extracted road pixels are inconsistent with the ground truth.

False Negative (FN): The areas where no roads are extracted are inconsistent with the ground truth.

These elements are illustrated in Figure 3-7.

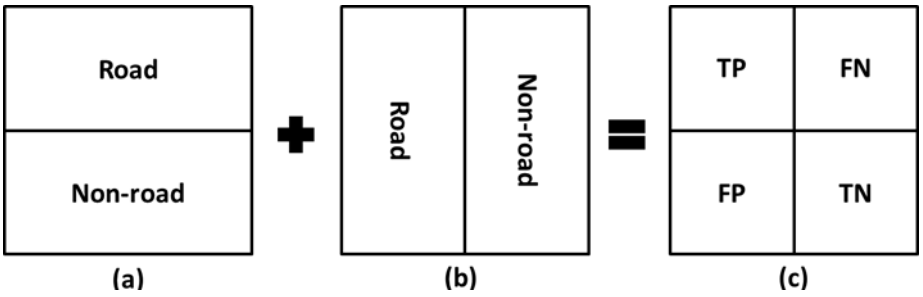

Figure 3-7 Illustration of quality elements: (a) Ground Truth, (b) Extracted roads, (c) Quality elements

Mathematical definition of quality measures is given below:

$$Precision = \frac{TP}{TP + FP} \tag{3.1}$$

$$Recall = \frac{TP}{TP + FN} \tag{3.2}$$

$$Accuracy = \frac{TP + TN}{TP + TN + FN + FP} \tag{3.3}$$

Table 3-3 provides an overview of the performance evaluation of classification results. A set of IKONOS multi-spectral images with 1-meter spatial resolution have been used. Training data for classification is selected manually. As can be seen from Table 3-3, both approaches are performing similar in most of images. However In some images GMM approach gives unsatisfactory results. This is due to the fact that the performance of GMM highly depends on the initialization of mixture components. A poor choice of initial parameters will cause poor results. From this point of view, OC-SVM algorithm provides a more robust solution. As we can see, the type of feature set used does not affect the result of OC-SVM algorithm very much. However, using less number of features is computationally more efficient.

Table 3-3 Quality Assessment of Spectral Classification using different methods and feature sets

Test Image	Method	Features	Precision (%)	Recall (%)	Accuracy (%)
Image 1	OC-SVM	PC1,PC2	52.3	91.7	96.0
	OC-SVM	R,G,B,NIR	65.0	90.8	97.5
	GMM	PC1,PC2	56.1	91.8	96.5
Image 2	OC-SVM	PC1,PC2	35.9	94.4	96.2
	OC-SVM	R,G,B,NIR	41.5	94.7	97.0
	GMM	PC1,PC2	13.1	95.1	86.3
Image 3	OC-SVM	PC1,PC2	28.5	87.5	88.6
	OC-SVM	R,G,B,NIR	31.3	91.8	89.7
	GMM	PC1,PC2	29.5	86.2	89.2
Image 4	OC-SVM	PC1,PC2	60.6	90.2	97.8
	OC-SVM	R,G,B,NIR	60.3	92.1	97.8
	GMM	PC1,PC2	51.6	97.3	97.0
Image 5	OC-SVM	PC1,PC2	31.8	93.8	92.2
	OC-SVM	R,G,B,NIR	39.7	92.2	94.4
	GMM	PC1,PC2	6.2	95.0	45.6

The output of classification algorithms for test image-1 is shown in Figure 3-8.

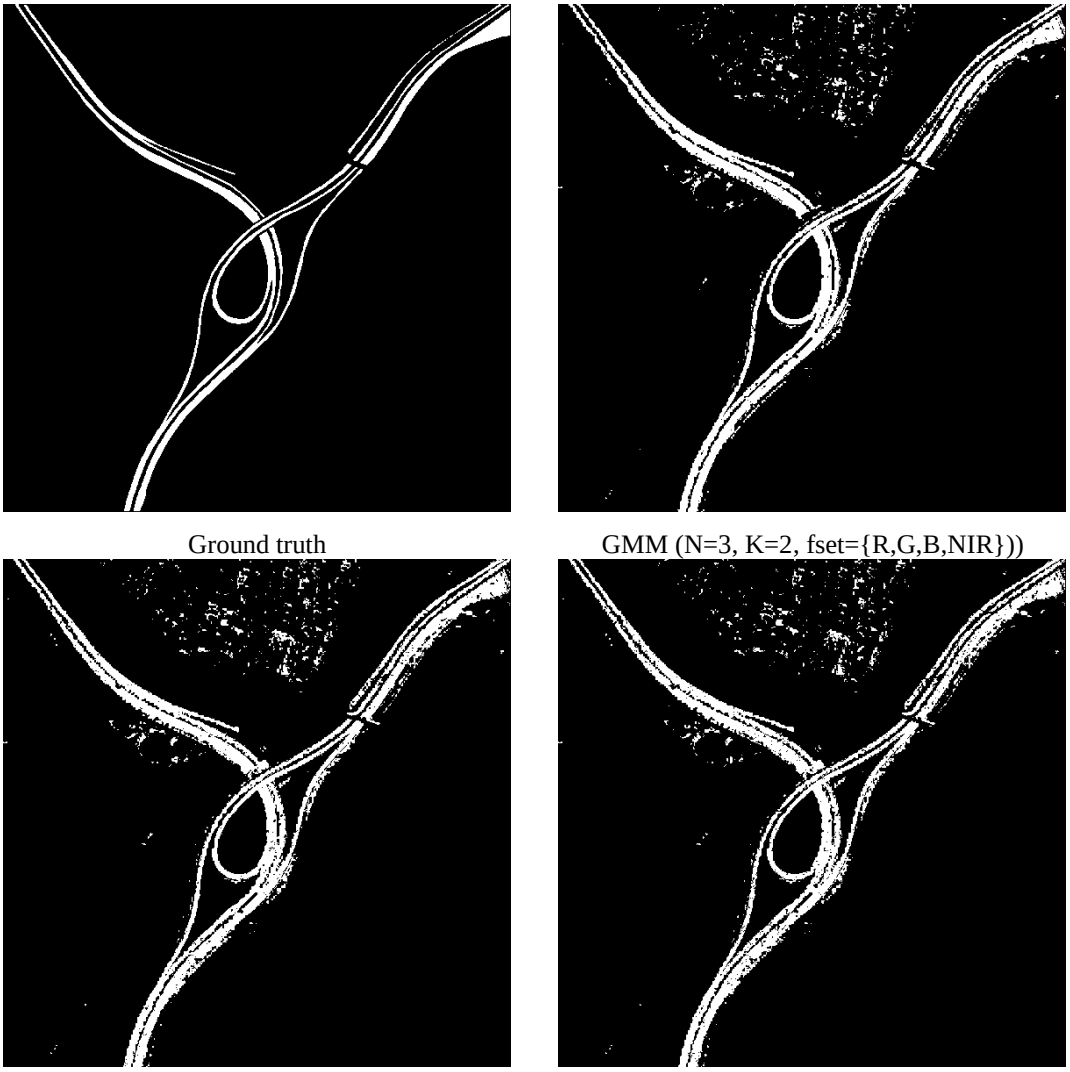

Ground truth | GMM (N=3, K=2, fset={R,G,B,NIR}))

OC-SVM ($\mathbf{v} = \mathbf{0.03}$, fset={PC1,PC2}) | OC-SVM ($\mathbf{v} = \mathbf{0.03}$, fset={R,G,B,NIR})

Figure 3-8 Classification results for test image - 1

Training set selection process can be automatized by Anti-parallel Centerline Extraction (ACE) algorithm described in Section 2.3. Road seed produced automatically by ACE is presented in Figure 3-9.b. These seed points are used to train the classifiers, OC-SVM and GMM with $feature\ set = \{PC1, PC2\}$. The classification results are shown in Figure 3-9.c and d respectively. Most of the roads are extracted with a satisfactory accuracy for this particular image (Table 3-4).

Table 3-4 Result of unsupervised classification

	OC-SVM	GMM
Precision	77.5	77.0
Recall	56.7	59.2
Accuracy	48.7	50.3

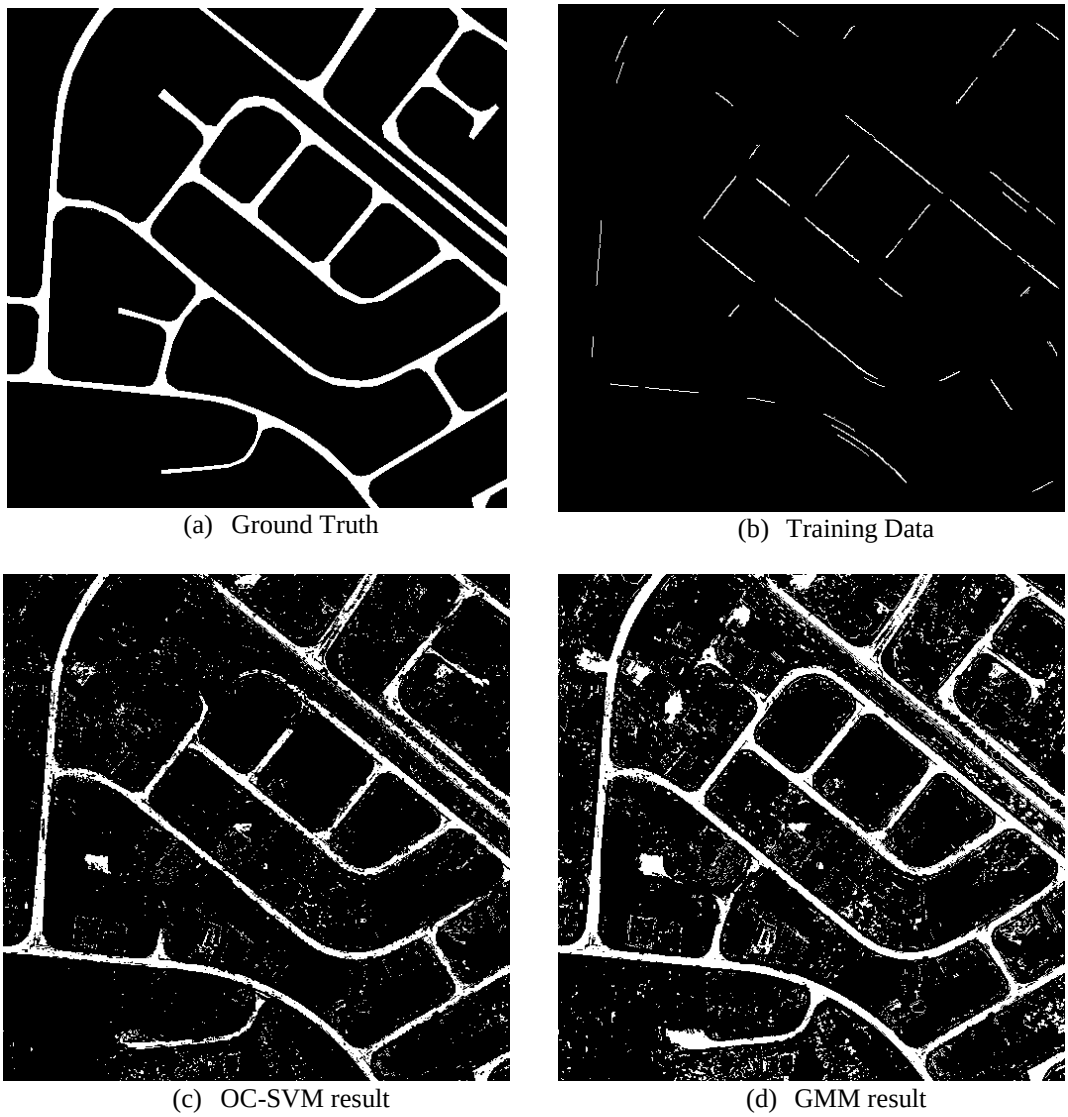

(a) Ground Truth (b) Training Data

(c) OC-SVM result (d) GMM result

Figure 3-9 Automatic Classification of Roads

3.3 Road Class Refinement

Although Multi-spectral images have very rich spectral information, the accuracy of classification results is not very satisfactory in some images due to the misclassification of objects other than roads such as parking lots, buildings, crop fields, etc. which have similar spectral signature with roads. In order to remove these misclassified regions, the structural properties of roads should also be taken into account.

A road segment appears as an elongated rectangular region in High Resolution Satellite Imagery. Based on this distinctive structure of roads, we present a road-model based technique to get rid of the regions misclassified as road. It is called Template Match Filtering.

3.3.1 Template Matching Filter

Template Matching Filter (TMF) is a set of directional rectangle filters which is proposed to remove open areas. A Satellite image may contain roads which have different widths and a template filter is constructed based on a specific target road width. Therefore, scaled versions of the original filter are used to detect different road widths. The minimum and maximum road width thresholds need to be determined. We have set these values to 7 and 15 pixels respectively for 0.5 meter spatial resolution satellite images. Since roads can be in any direction, rotated versions of these filters are also generated. This makes the filtering result rotation-invariant.

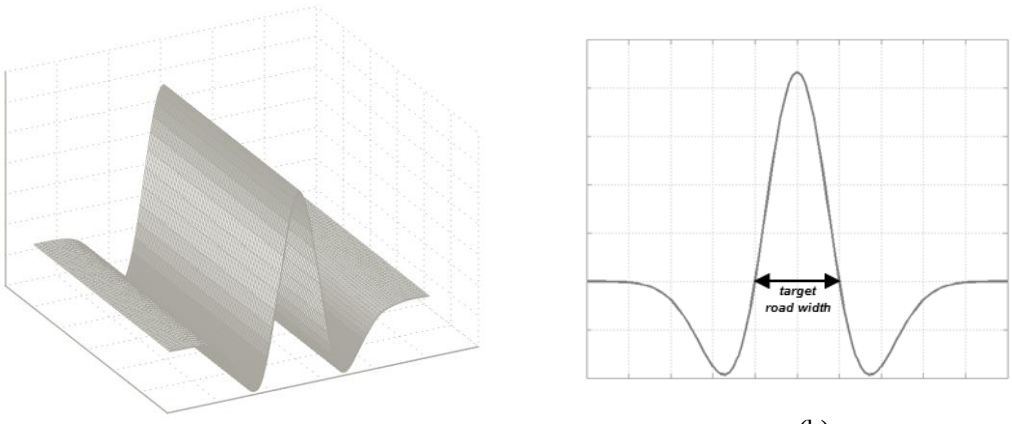

(a) (b)

Figure 3-10 Template Matching Filter: (a) filter structure in 2D, (b) cross-section of filter

The structure of Template Matching Filter (TMF) is illustrated in Figure 3-10. The distance between the zero crossings of the filter cross-section indicates the target road width (Figure 3-10.b).

All these filters are applied to each pixel in the classified image and the value of pixel is replaced by the maximum response obtained from these filters. The response of rotated-filters for a specific road is shown in Figure 3-11. In Figure 3-11.b and c, there is a peak at location around 90^{o}. This represents the direction of road.

Filtering process is repeated n times. At each iteration, elongated regions emphasized more and more, at the end only regions which perfectly match with the filter structure remain. Applying filter iteratively also has an effect on filling the gaps on roads and removing the irregularities on the road borders.

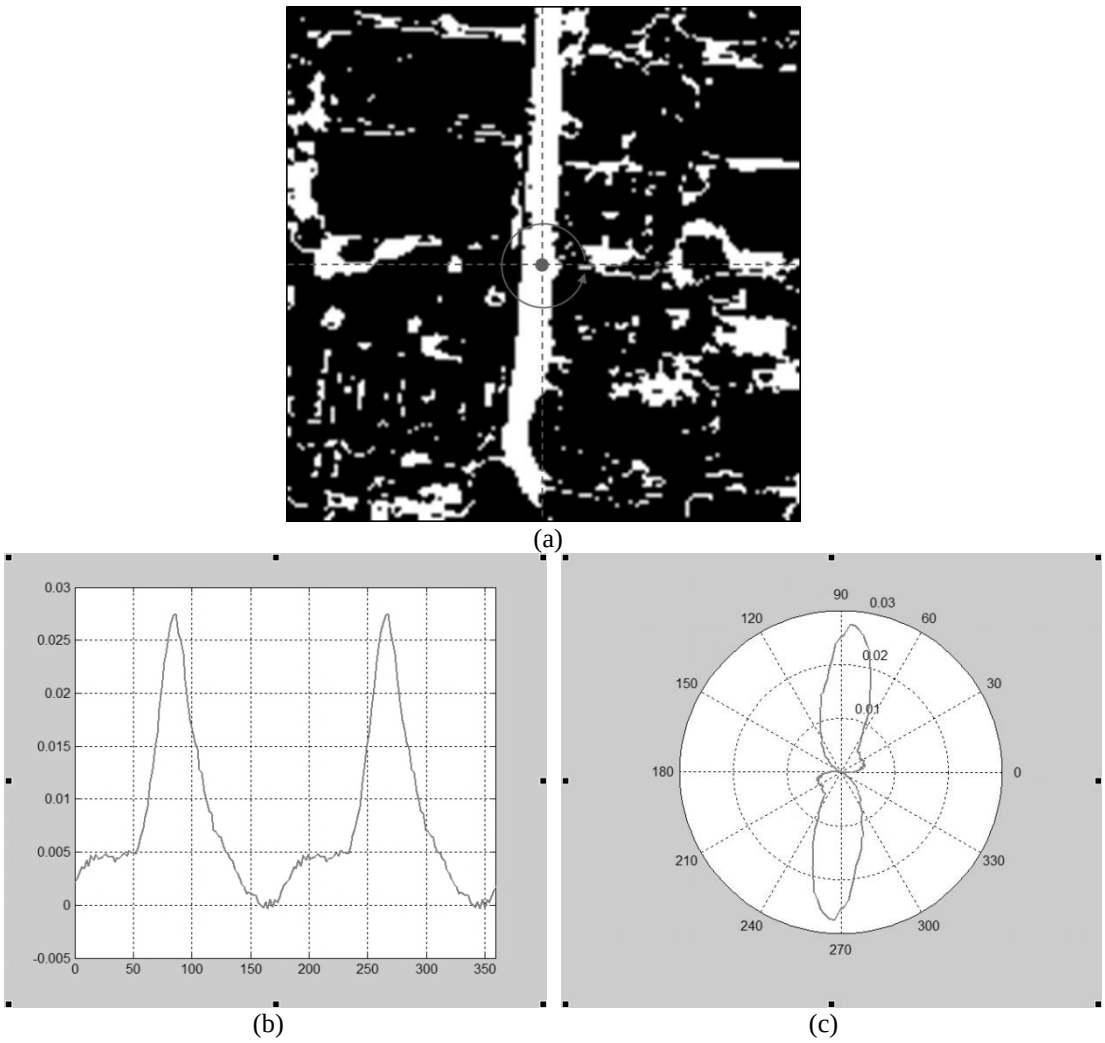

Figure 3-11 Template Matching Filter Response: (a) Original image, (b) Filter response (linear plot), (c) Filter response (polar plot)

As it can be seen in Figure 3-12, the roads become more and more emphasized at each iteration and small segments are disappearing gradually. We can see also that the gap filling effect of filtering at several locations. Generally, 4-5 iterations are sufficient. After then, the effect of filtering becomes insignificant. After template matching filter is applied, the classification result which is based on the spectral features of roads is combined with structural features of roads to increase classification accuracy.

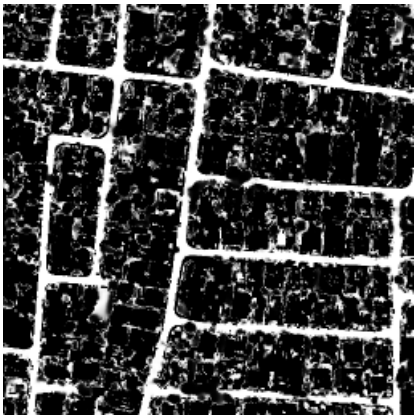

Input classified image

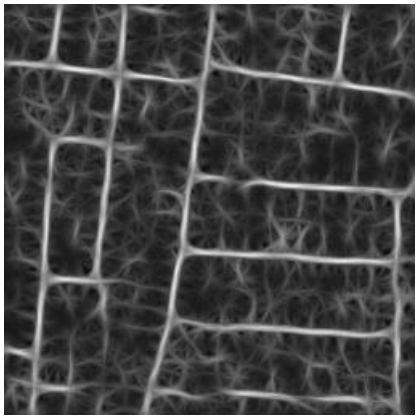

Iteration 1

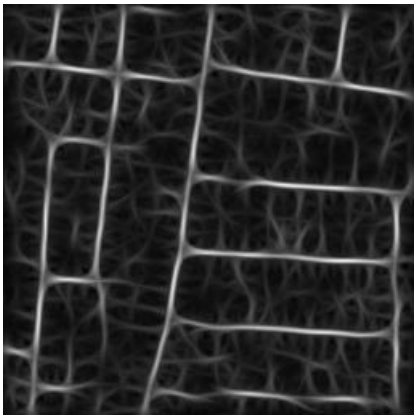

Iteration 2

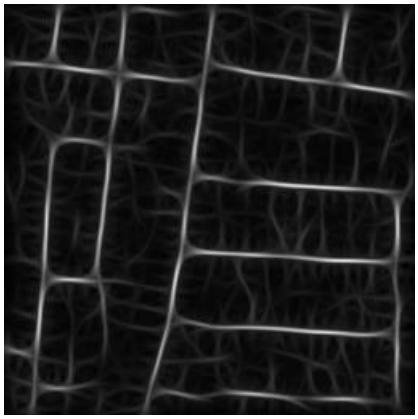

Iteration 3

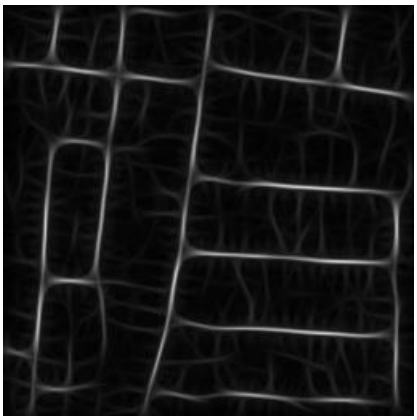

Iteration 4

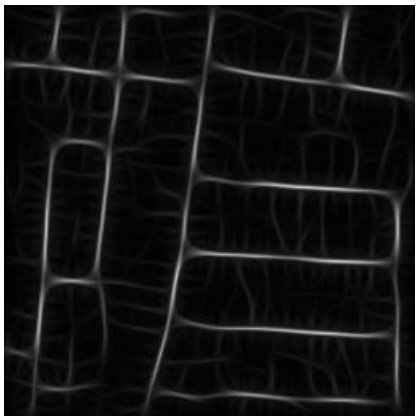

Iteration 5

Figure 3-12 Template Matching Filter Outputs

3.4 Road Centerline Extraction

In this work, Self-Organized Road Mapping (SORM) by Doucette is used for the purpose of binary clustering. K-Medians approach in SORM technique is adapted in order to cluster the spectrally classified image. Cluster centroids are treated as candidate roads center-points, and in the next section, they will be used to construct road network.

After filtered image is obtained, two different approaches can be employed to extract candidate road center points. These approaches are presented in Figure 3-13.

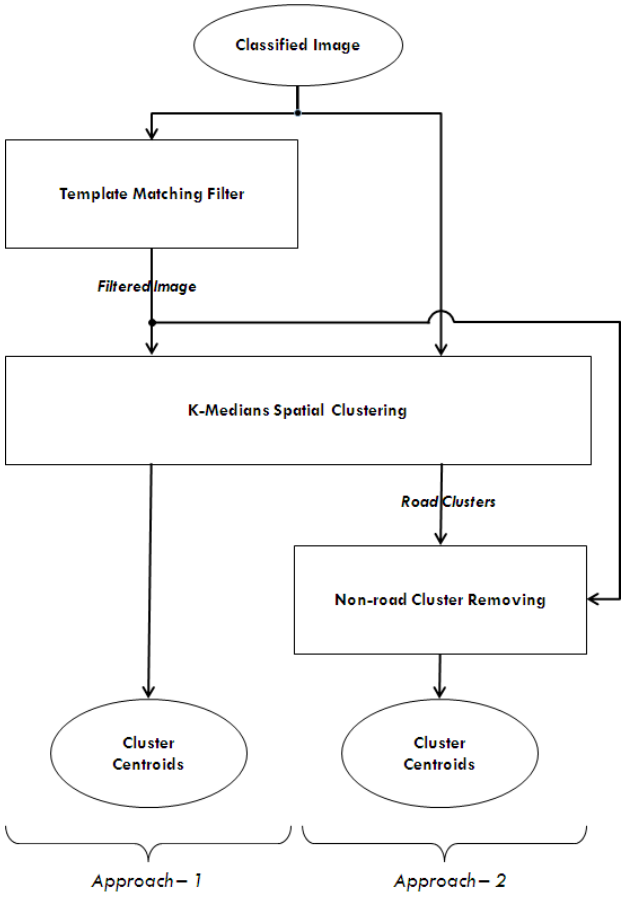

Figure 3-13 Flows of Centerline Extraction Algorithms

a. First Approach:

K-Medians clustering can be applied directly on the filtered image. Since a binary image needs to be provided as an input to K-medians clustering, the filtered image is converted to a binary image with a proper threshold value. These clusters' centroids represent the candidate road centerline points.

b. Second Approach:

Alternatively, original image is clustered by K-Medians first. Then, filtered image is used to remove non-road clusters. The remaining cluster centroids represent candidate road centerline points. Non-road cluster removing can be done easily by computing the average response in filtered image within the boundary of cluster. If the response is less than a predefined threshold, cluster is removed. In this way, original road structure (e.g. road width information) is preserved.

Centerline points extracted by these two approaches are shown in Figure 3-14. As we can see in Figure 3-14.b, the classification accuracy of this particular image displayed in Figure 3-14 is not very high. There are a lot of noises and some occluded regions on road network. The results obtained by approach-1 and approach-2 are displayed in Figure 3-14.c and Figure 3-14.e respectively. Both approach gave satisfactory results, and succeeded to remove most of the misclassified regions. However, the result of first approach is smoother and less noisy than the other. When comparing location of the cluster centroids (Figure 3-14.d and Figure 3-14.f), it is observed that the first approach achieves better results. In the second result, at several locations, clusters centroids are departed from actual road centerline because of noise on the road boundaries. This will cause the final road network not to match perfectly with actual road network. Therefore, first method is more suitable for network extraction problems and we will continue with this method.

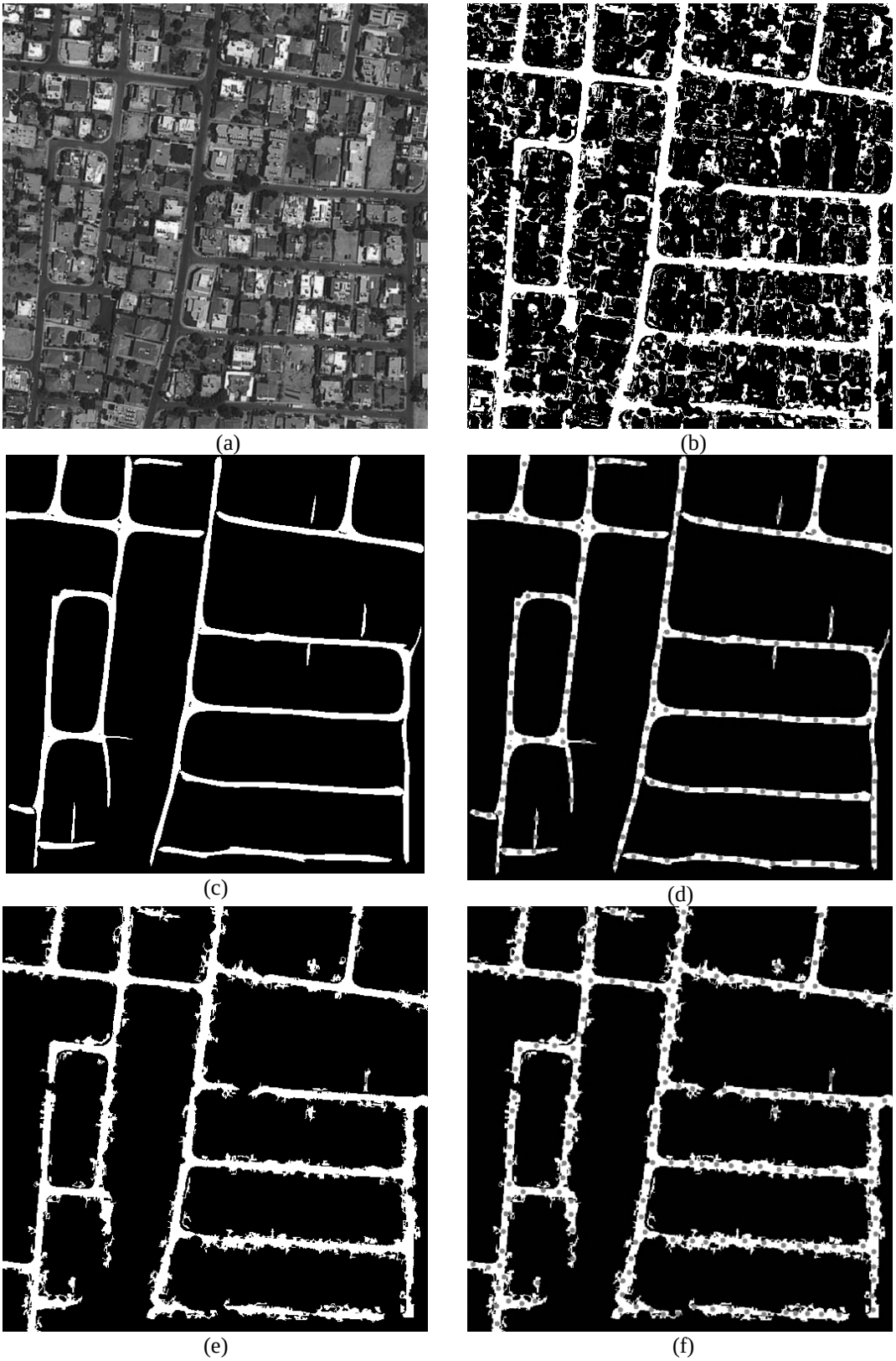

Figure 3-14 Road Centerline Extraction: (a) Original Image, (b) Classified Image, (c) Output of first approach, (d) Cluster centroids obtained by first approach, (e) Output of second approach, (f) Cluster centroids obtained by second approach

Classification result can also be used directly without applying any of these road class refinement procedures. However, in this case there will be excessive amount clusters centroids due to noise and open areas which are not part of road network. This will cause the road network formation procedure in the next chapter takes too long and even generates unsatisfactory results. Therefore, eliminating the false detected centerline points simplifies the Road network formation step.

The next section is dedicated to establishment of the final road network from road centerline points obtained.

3.5 Road Network Formation

The methods presented in the previous section extracts the possible road centerline points. Without any further processing these points are just randomly distributed points in image space with no relation between them. This section tries to find the contextual relationships between these points to construct a road network.

The aim of Road network formation step is to link individual road objects into meaningful road network. In this work, we employ a Markov Random Field to model context dependencies between individual road center-points for the purpose of road network reconstruction.

This section is organized as follows: First the MRF model of our network extraction problem is provided. Then, the energy function of MRF is defined. In the section following it, the details of energy minimization technique are provided. Finally, we will focus on some post-processing techniques to improve results.

3.5.1 Markov Random Field

Basic principles of Markov Random Fields are explained in the section 2.6. Now, we employ a Markovian framework for grouping the road centerline points. The centerline points are derived via K-medians clustering algorithm in section 0. Markovian model for road-like objects are adopted from the earlier work of Tupin et al. (1998) where they propose a two-step procedure to detect main axes in road networks in synthetic aperture radar (SAR) images. The first step is local and is used to extract the linear features and in the second step, which is global, a Markov Random Field is defined on a set of segments which is composed of the detected segments in the first-step and additional segments connecting the previous ones. Then the segments are used to build MRF graph and the road network extraction is achieved by the estimating the best graph labeling based on a MRF model for road like structures and a maximum a posteriori probability (MAP) criterion.

In our problem, we used MRFs to label a graph describing relationships between centerline points. Defining Markov random fields onto this graph, associated with an energy function of road networks, leads to the expression of road network extraction as a global energy minimization problem. Our MRF Energy function definitions are similar to one in Tupin's paper with some modifications on it.

3.5.1.1 Graph Creation

The road centerline points produced in the previous chapter is used to build a MRF graph. The nodes of the graph are the set of all possible connections between the centerline points. These possible connections are extracted based on distance criteria. In other words, two points connected with a line segment if the distance between them is less than a certain specified threshold d_{max}. This threshold value highly depends on the grid spacing and the minimum distance parameters used in K-Medians algorithm. It is obvious that, d_{max} should be greater than the grid spacing, and for poor detection rates this value should be at least 2 or 3 times the grid spacing. However, using very high threshold values increase the number of connections dramatically, and it may cause to increase the optimization time and also the chance of trapping in the local minima of energy function.

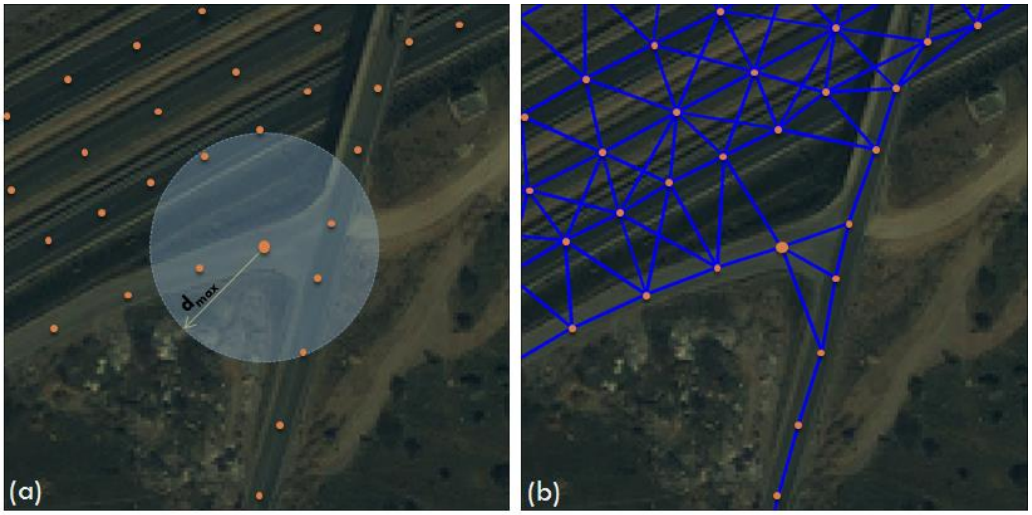

Figure 3-15 (a) Road Centerline points obtained by using SORM Algorithm and (b) Candidate Road Segments connecting these centerline points based

Each line connecting two centerline points (i.e. cluster centroids) represent a node in segment graph. Among these segments, some of them belong to actual road network, but others do not.

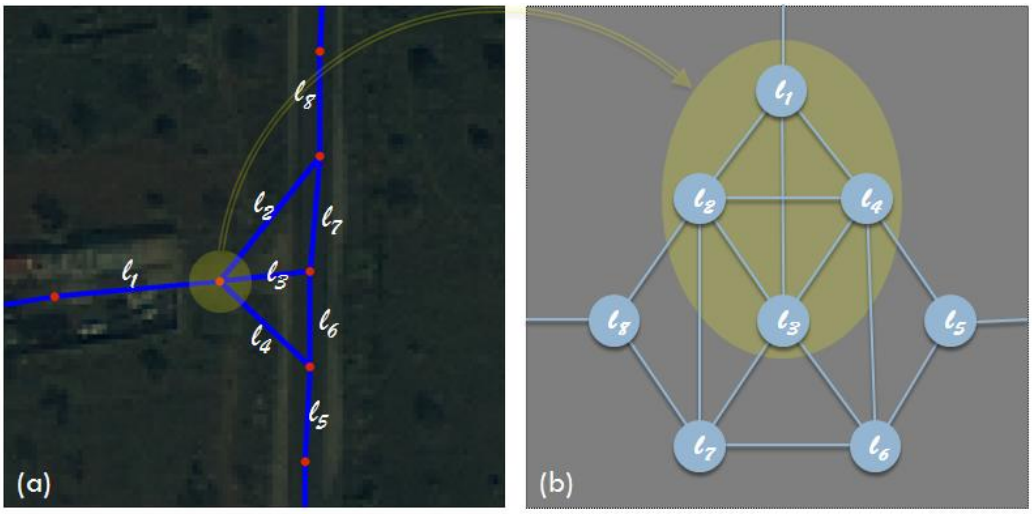

Figure 3-16 (a) Candidate road segments, (b) graphical representation of road segments

The set S containing all the segments connecting candidate road center-points is organized as a graph $G = (S, A)$.

Each node $i \in S$ which corresponds to the segment connecting two centerline points is associated with a normalized segment length ($l \in [0,1]$) and an observation value $d_i \in [0,1]$ which is the average road detection response value along the segment. The observation value is computed by putting a window around the segment and determining the average response within that window in classified image (Figure 3-17). To each $A_{ij} \in A$ between nodes i and j in MRF graph is associated the angle $\theta_{ij} \in [0, \pi]$ which is the smaller angle between the two segments.

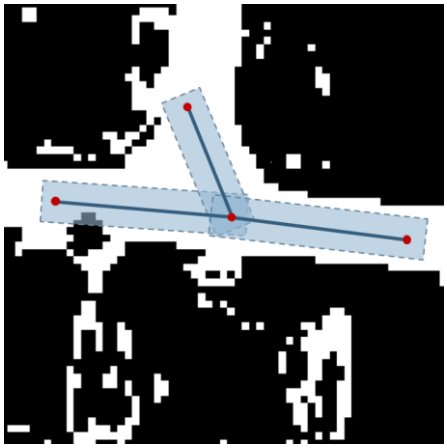

Figure 3-17 Computation of observation value

In order to define a MRF on a segment graph, the neighborhood N_i of each node i is defined by

$$N_i = \{j \in S | \exists (k,p) \in \{1,2\}^2, M_j^k = M_i^p, j \neq i\} \quad (3.1)$$

where $M_j^k for\ k \in \{1,2\}$ denote the endpoint of a segment j.

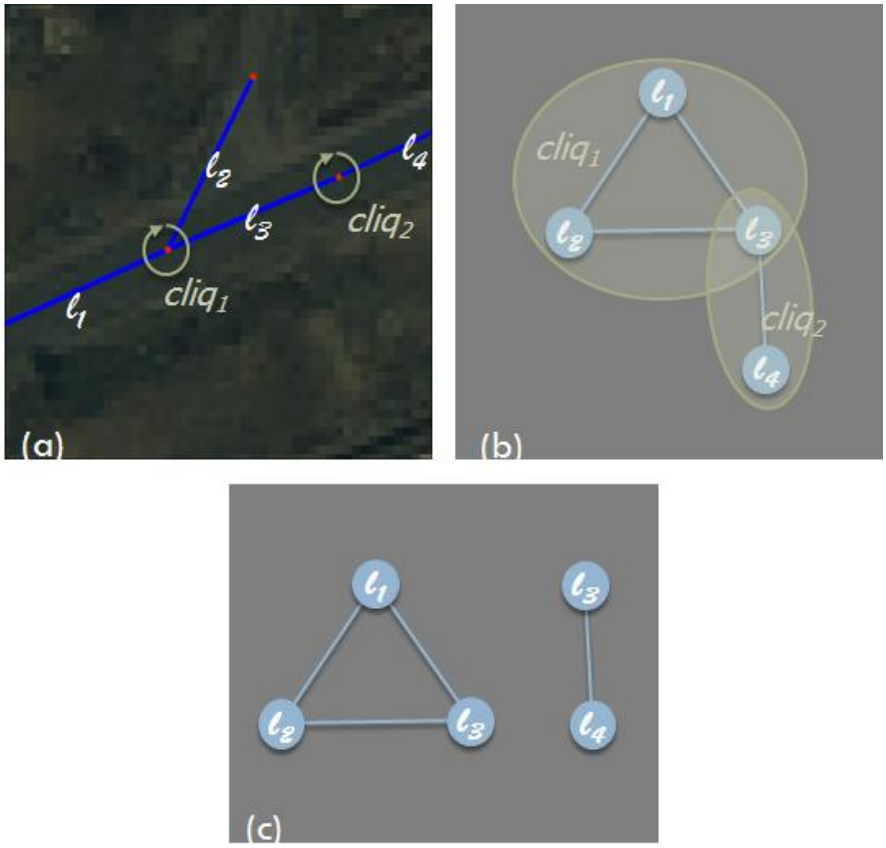

Figure 3-18 (a) Candidate road segments, (b) graphical representation, (c) maximal clique set

The Cliques of the graph G are all subsets of segments sharing a cluster centroid. In our graph definition, each center-point actually represents a clique in MRF graph. This relation is illustrated in Figure 3-18.a and b. There are two intersection points $cliq_1\ and\ cliq_2$ which are connecting segments $\{l_1, l_2, l_3\}$ and $\{l_3, l_4\}$ respectively. These segment sets represent the cliques of MRF graph. It can be easily shown that set of all segments connecting center-points gives maximal clique set of the graph. Finding the maximal clique set is important because MRF energy function is expressed in terms of clique potentials. Energy function definition will be provided in the following section.

After MRF Graph is built, extraction of Road Network problem is transformed into graph labeling problem. Now, our aim is to find the most probable configuration for L given the observation process D for the segment of S with a *maximum a posteriori* (MAP) criterion. In other words, the solution corresponds to the maximum of the posterior probability distribution $p(L|D)$. Using Bayes rule

$$p(L|D) = \frac{p(D|L)p(L)}{p(D)} \tag{3.2}$$

where $P(L)$ is the prior probability of labeling L, $p(D|L)$ is the conditional probability distribution function of the observation process D. $p(D)$ is a constant which does not depend on the realization of L. As a result, instead of the posterior probability distribution $p(L|D)$, the prior and the conditional probability distributions, $P(D)\ and\ p(D|L)$, have to be estimated.

3.5.1.2 Energy Function Definition

The conditional probability distribution of the observation field $p(D|L)$ stems from a supervised learning step on known areas, and the a priori probability distribution $p(L)$ relies on a Markovian model of usual roads.

Conditional Probability Distribution $p(D|L)$:

$p(D|L)$: Let us first define the observation process $D = (D_1, D_2, \dots, D_N)$ calculated from the spectrally classified image. Average response along the road segment gives the observation d_i associated to i. Assuming that the observations D_i are independent and the conditional probability distribution of D_i only depends on L_i, we may write

$$p(D|L) = \prod_{i=1}^{N} p(D_i|L) = \prod_{i=1}^{N} p(D_i|L_i) \tag{3.3}$$

By defining $P(D_i|L_i) = \exp[-V(d_i|l_i)]$, where $V(d_i|l_i)$ denotes the potential of segment i.

$$V(d_i|l_i) = -\ln(p(D_i|L_i)) \tag{3.4}$$

Conditional probability distribution is directly related to observation value obtained from classified image. Therefore, it can be defined simply as:

$$p(D_i = d_i|Li = 0) = 1 - d_i \tag{3.5}$$

$$p(D_i = d_i|L_i = 1) = d_i \tag{3.6}$$

That is to say, if a segment is labeled as road ($i.e.\ l_i = 1$), conditional probability distribution is equal to the observation value of that segment. On the other hand, if it is labeled as non-road segment (i.e., $l_i = 0$), conditional probability distribution is equal to ($1 -$ observation value).

By combining these two statement segment potentials can be expressed in a closed form as follows,

$$p(D_i = d_i | L_i = l_i) = 1 - d_i - l_i + 2l_i d_i \tag{3.7}$$

$$V(d_i | l_i) = \ln(1 - d_i - l_i + 2l_i d_i) \tag{3.8}$$

Prior Distribution $p(L)$:

According to the Hammersley-Clifford theorem which is stating the equivalence of MRF and Gibbs distributions, the joint probability $P(L = l)$ can be expressed in terms of the clique potential functions $V_c(l)$.

$$p(L = l) = \frac{1}{Z'} \exp[-U(l)] \tag{3.9}$$

where Z' is a normalizing constant, C denotes the clique set, and $U(l) = \sum_{c \in C} V_c(l)$.

Clique potentials should reflect the following three main a priori knowledge about roads:

i. Roads are long structures
ii. Roads have a low curvature
iii. Intersections between roads are rare

Clique potentials are defined as in the work of Tupin et al. (1998)

i. $V_i \in c, l_i = 0 \Rightarrow V_c(l) = 0$

ii. $\exists!\, i \in c | l_i = 1 \Rightarrow V_c(l) = K_e - K_L L_i$

iii. $\exists!\, (i,j) \in c^2 | l_i = l_j = 1, R_{ij} > \frac{\pi}{2} \Rightarrow V_c(l) = -K_L(L_i + L_j) + K_c sin R_{ij}$

iv. $in\ all\ other\ cases \Rightarrow V_c(l) = K_i \sum_{i | i \in c} l_i$

There are four parameters (K_e, K_L, K_c, K_i) available. They have to be chosen accordingly in order to fulfill the three road characteristics given above.

Posterior Distribution $p(L|D)$:

Since $p(D|L)$ and $p(L)$ correspond to Gibbs distributions defined on the same graph, so does the global-filed probability distribution (Tupin et al., 1998). Therefore $L|D$ is a MRF defined on graph G with global energy given as follows:

$$U(l|d) = \sum_{i=1}^{N} V(d_i | l_i) + \sum_{c \in C} V_c(l) \tag{3.1}$$

$$U(l|d) = \sum_{i=1}^{N} -lnP(d_i | x_i) + \sum_{c \in C} V_c(l) \tag{3.2}$$

The first energy term models a priori knowledge about roads which is obtained from the spectral classification of image. This term does not contain any information about the structure of road networks. The second term, however, models the contextual features of a road network. Combination of these two terms gives a complete model for a road network.

As a result, we have obtained a global interpretation of road network based on Markov Filed defined on a set of segment connecting candidate road centerline-points. Now, our aim is to find an optimum label set that minimizes the energy function. The optimization method to find a MAP configuration corresponds to minimum energy will be provided in the next section.

3.5.2 MRF Model Optimization

In order to find an optimum solution for road network problem, we need to find the label set which corresponds to minimum energy. Finding the exact MAP estimation is computationally very expensive. Therefore some approximation methods will be used to estimate it. Since the energy function is non-convex, deterministic optimization algorithms will not work. So, a stochastic minimization algorithm has to be chosen to find a global solution. Simulated Annealing algorithm will be used in this work.

The Simulated Annealing algorithm is a probabilistic method proposed in (Kirkpatrick, Gelatt Jr., & Vecchi, 1983) and (Černý, 1985) for finding the global minimum of a cost function that has several local minima. This algorithm models the physical process heating a material and then slowly lowering the temperature to decrease defects, thus minimizing the system energy.

In order to use simulated annealing algorithm, we must generate a realization of the label process l. Since the conditional distribution of MRF is very complicated, it is not possible to sample Markov Random Fields directly. Therefore iterative methods are used. The Metropolis Sampler and the Gibbs sampler is commonly used sampler for MRFs. The idea behind using iterative samplers is that the iterant will converge to samples representative of the distribution. We have used Gibbs sampler to generate samples from the conditional distribution of MRF.

The Gibbs Sampler was first introduced by Geman & Geman (1984). The method can be summarized as follows: one sweep through the MRF graph updating one node at a time. At each step, a node is updated to be a random draw from its conditional distribution while holding all neighboring nodes fixed.

The stochastic optimization using Simulated Annealing takes a long time. For a large number of nodes, this time increases dramatically. Alternatively, we may also use deterministic algorithms, like iterated conditional modes (ICM). Although these algorithms have the drawback of converging to local minima, we can achieve some results close to the global minimum results with a good initial labeling. For instance, all the segments which have an observation value above a threshold are labeled one, while the others are labeled zero. For such an initialization, it can be assumed that we are very close to global minimum.

Iterated Conditional Modes (ICM) is an optimization method for finding suboptimal solutions. It was first presented by Besag (1986). ICM algorithm updates the labels at one site at time. The new label for a site is chosen so as to maximize the energy for which all other sites are held constant. This iterative method converges to a local minimum depending on the chosen initialization rather than a global minimum.

Road network extraction results obtained with these two optimization techniques are shown in Figure 3-19. With ICM, we have obtained a result very close to the one obtained with Simulated Annealing optimization, but it is not optimum because it converge to a local minima rather than global minima. Figure 3-20 shows two network locations where Simulated Annealing has performed better. According to the MRF energy, the connection schemes in Figure 3-20.a and c has a lower energy value than the ones in Figure 3-20.b and d.

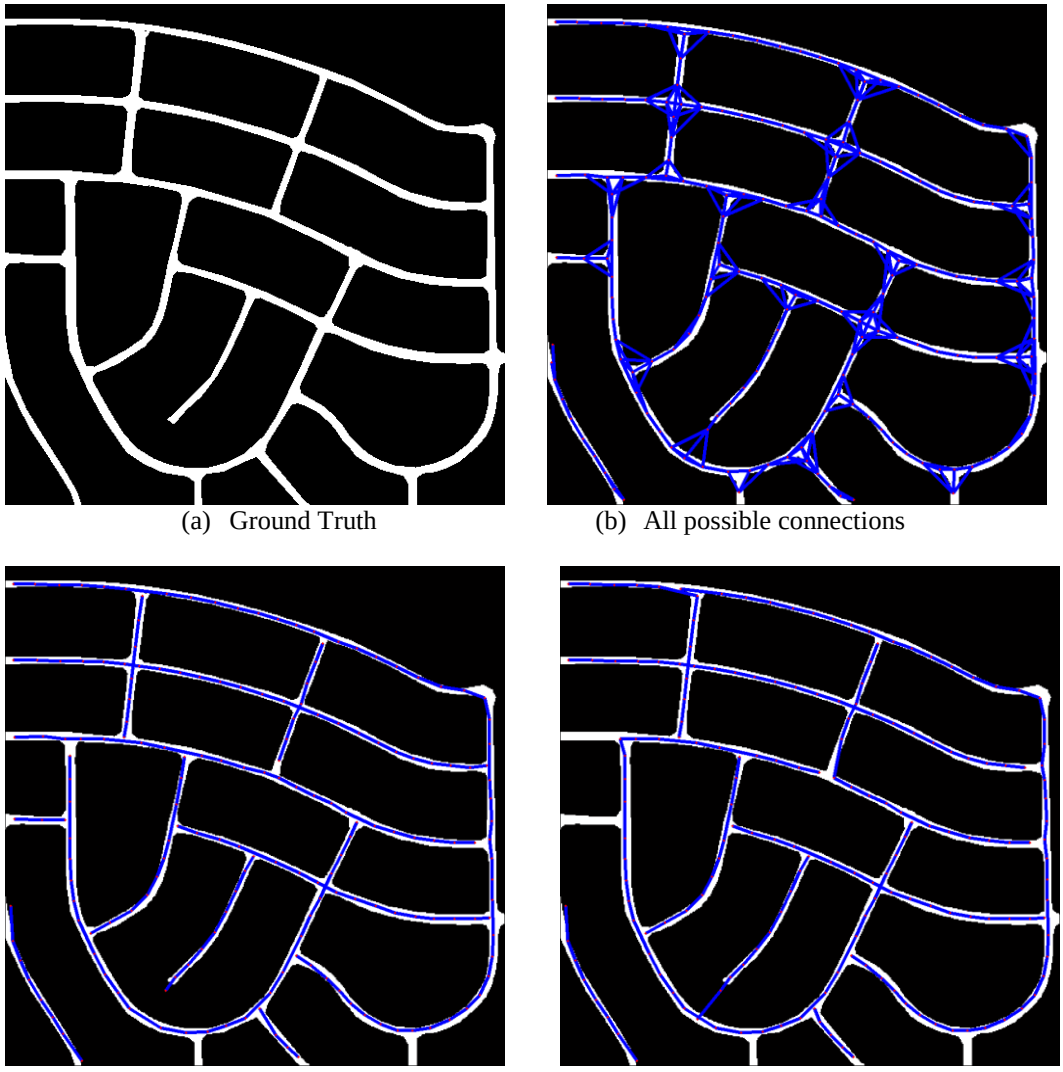

(a) Ground Truth (b) All possible connections

(c) Optimum connections (SA) (d) Optimum connections (ICM)

Figure 3-19 Road Network Extraction

Most of the road network has been extracted with a satisfactory accuracy. However, T-shape junctions are generally not detected. In the next section, a post-processing technique will be discussed to connect these T-junctions.

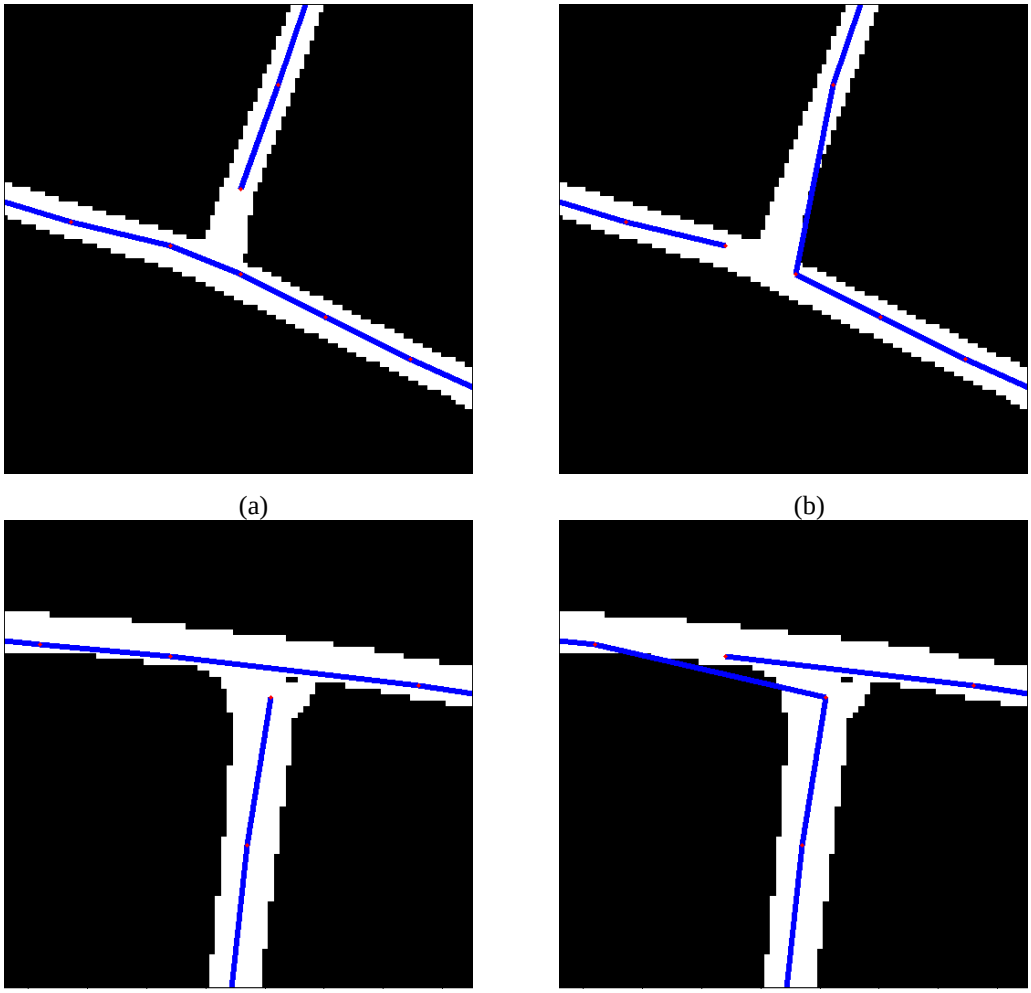

(a) (b)

(c) (d)

Figure 3-20 Simulated Annealing (a, c) vs. ICM (b, d)

3.5.3 Post Processing with Modified Energy Function

Since the Clique potential function defined previously gives road intersections lower probability than the connection between only two segments, most of the road intersections were missed. In order to detect these intersections also, the definition of Clique Potential function is modified. Another case has been added to potential function definition to detect T-shape junctions.

i. $V_i \in c, l_i = 0 \Rightarrow V_c(l) = 0$

ii. $\exists! \, i \in c | l_i = 1 \Rightarrow V_c(l) = K_e - K_L L_i$

iii. $\exists! \, (i,j) \in c^2 | l_i = l_j = 1, R_{ij} > \frac{\pi}{2} \Rightarrow V_c = -K_L(L_i + L_j) + K_c sin R_{ij}$

iv. $\exists! \, (i,j,k) \in c^3 | (l_i = l_j = l_k = 1), \ \left(R_{max} > \frac{\pi}{2}\right) \Rightarrow$

$$V_c(l) = -K_L(L_i + L_j + L_k) + \frac{K_c}{2}\left(sin(R_{max}) + \sin\left(\frac{R_{mid} - R_{min}}{2}\right)\right)$$

v. $in\ all\ other\ case\ V_c = K_i \sum_{i|i \in c} l_i$

Here the function defined in (iv) is new. It gives the minimum energy when a perfect T-junction ($i.e., R_{max} = \pi, R_{mid} = R_{min} = \frac{\pi}{2}$) is detected. Figure 3-21 gives an instance of a clique that only include segment i, j, k. If all segments related to this clique are labeled as road segment ($i.e., l_i = l_j = l_k = 1$) and maximum deflation angle between them is greater than $\pi/2$, the potential of this clique is calculated as given in the case iv.

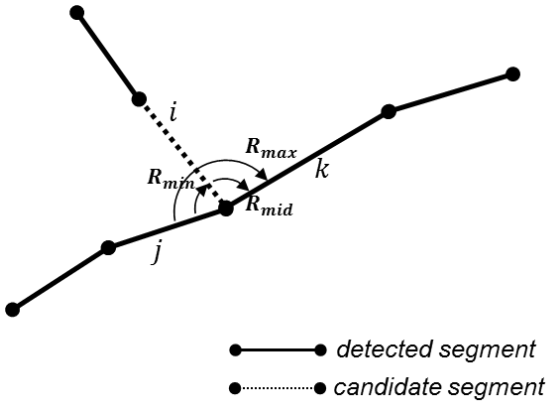

Figure 3-21 Road junction detection

All the unconnected endpoints in the extracted road network are analyzed to check whether it constructs a T-junction. As shown in Figure 3-22, Segment i can be connected to road network through segments 1, 2, and 3. For all these three configurations, new energy levels are computed. If the connection with minimum energy level decreases the previously obtained optimum energy level, this connection accepted and road network updated accordingly. There may not be a node located close to the junction point. Therefore, Results can be further improved by creating new nodes along the unconnected segment direction as shown in Figure 3-23.

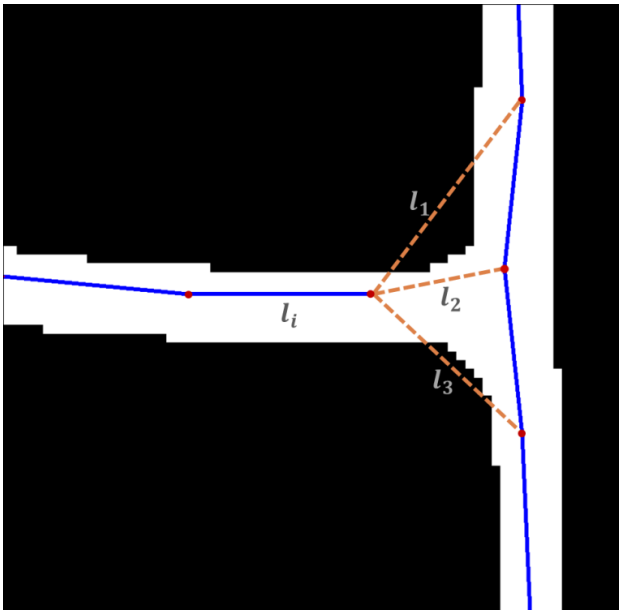

Figure 3-22 Post-processing: finding possible connection.

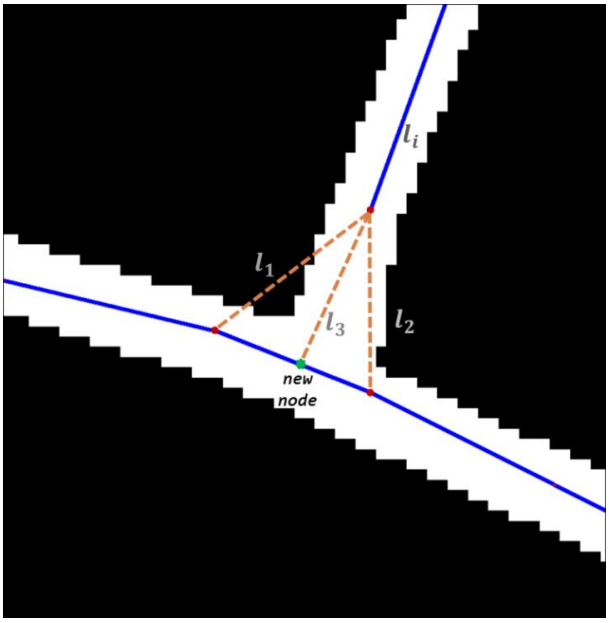

Figure 3-23 Post-processing: inserting new node.

Unconnected centerline points are also considered as endpoint as shown in Figure 3-24

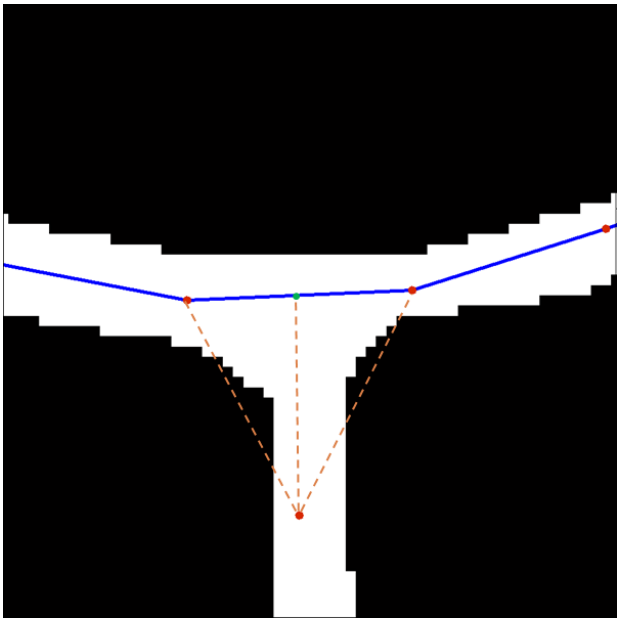

Figure 3-24 Post-processing: Handling unconnected centerline points.

Final road network after post-processing is illustrated in Figure 3-25. Although most of the roads are successfully extracted, there is a miss-localization problem of road main axis at some points where roads make curve. This is an inevitable effect of filtering used in road class refinement step.

The road network is not very smooth, since it is represented by small straight line segments connecting centerline points. The smoothness of roads can be improved by decreasing the grid spacing used in K-medians clustering. However, in this case, the number of segment will increase significantly and optimization time will increase. Therefore, there is a tradeoff between accuracy of road centerlines and network extraction time.

Figure 3-25 Final road network

The modified energy function can be directly used in the first optimization level. However, in this case, we observed that a lot of false junctions are extracted. Therefore, applying the original energy function first, then using the modified energy function in a second optimization stage is gives better results.

3.6 Conclusion

We have demonstrated a complete road network extraction system in this chapter. This system combines a number of different algorithms to extract roads from high resolution multi-spectral images. Output of each system stage is presented. In the next chapter, the performance of full extraction framework will be evaluated by defining a set of quality metrics.

CHAPTER 4

QUALITY ASSESSMENT

In this chapter, the quantitative performance analysis of the proposed road network extraction algorithm will be assessed based on the results obtained on three test images from Google Earth. Results for IKONOS test images are given in Appendix A. The images have three spectral bands (red, green and blue) with 1m spatial resolution. The performance of proposed extraction algorithm is evaluated by comparing the extracted road network with the manually generated reference road network. The main problem with the quality assessment is to locate all the matching road segment pairs from two versions of a road network, extracted versus reference. This process is done manually, which is very time consuming.

Sections of this chapter are organized as follows: Section 4.1 introduces the quality metrics used in this study. Section 4.2 discusses the evaluation results of proposed road network extraction system. Section 0 summarizes the chapter.

4.1 Quality Metrics

In the previous chapter, a visual comparison of the extracted roads with reference roads shows that most of the roads have been extracted successfully. However, we do not know exactly the number of missed roads, false roads and shifted roads. Therefore a quantitative assessment of results is necessary. Several quality metrics are available in the existing literature. The measures to be used in this study for evaluating performance of results produced by road network extraction system are chosen as completeness, correctness, quality and root mean square error (RMSE) as presented by Wiedemann (2003).

4.1.1 Completeness

The completeness is defined as the ratio of the extracted road data matched with the reference road data to the total length of the extracted road network. The correctness has a range of [0, 1].

The completeness metric is calculated as

$$Completeness = \frac{length\ of\ the\ matched\ reference}{length\ of\ reference} \tag{4.1}$$

where $completeness \in [0,1]$. The completeness is a measurement of the percentage of the reference data which is explained by the extracted data, i.e., the percentage of the reference network which could be extracted. A completeness value of one indicates that the reference network is entirely covered by the buffer area around the extracted network. A visual explanation of completeness is given in Figure 4-1.a.

4.1.2 Correctness

The correctness is defined as the ratio of the extracted road data matched with the reference road data to the total length of the extracted road network. The correctness metric is calculated as

$$Correctness = \frac{length\ of\ matched\ extraction}{length\ of\ extraction} \tag{4.2}$$

where $correctness \in [0,1]$. A correctness value of 1 indicates that the extracted network is entirely covered by the buffer area around the reference network. The correctness represents the percentage of correctly extracted road data, i.e., the percentage of the extraction, which is in accordance with the reference. A visual explanation of correctness is given in Figure 4-1.b.

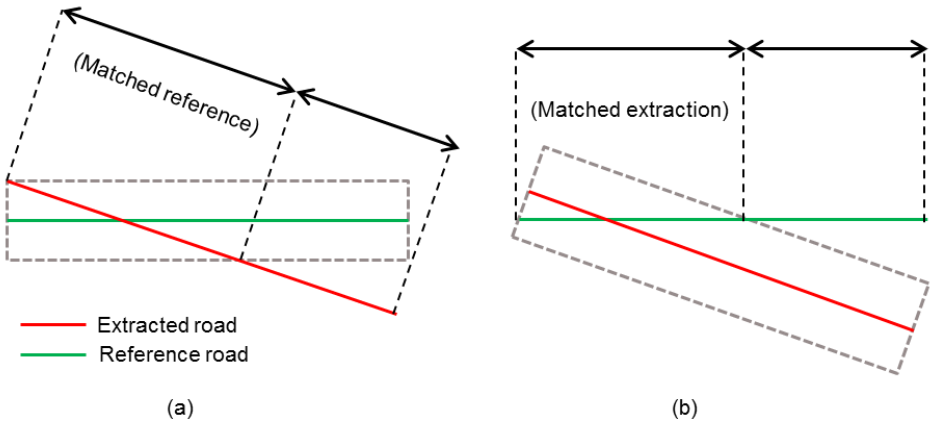

Figure 4-1 True and false extractions: (a) Completeness, (b) Correctness

4.1.3 Quality

Quality is a measurement that combines completeness and correctness. The quality metric is calculated as

$$Quality = \frac{Completeness.Correctness}{Completeness - Completeness * Correctness + Correctness} \tag{4.3}$$

where $Quality \epsilon [0,1]$. A quality value of 1 indicates that the extracted network lies within the buffer around the reference network and also vice versa. Quality is a normalized measure between completeness and correctness. The quality value can never be higher than either the completeness or correctness measurement.

4.1.4 Root mean square differences (RMSE)

The RMSE defines the average distance between the extracted road network and corresponding matched reference. It expresses the geometrical accuracy potential of the extracted road data and is usually calculated using the following equation:

$$RMSE = \sqrt{\frac{\sum_{i=1}^{K} d(ext_i, ref)^2}{K}} \tag{4.4}$$

where $RMSE \in [0, b]$. The parameter K is defined as the number of matched line segments and $d(ext_i, ref)$ is the distance between the i^{th} segment of the extracted line and its corresponding reference line. The optimal value for RMSE is 0, indicating that the extracted road lies on the top of the reference set. The maximum value depends on the size b of the buffer zone.

The distance between the extracted road segment and the associated reference road segment is calculated by projecting the endpoints of matched portion of the extracted road segments onto the reference road segment. Then the average distance $d = (d_1 + d_2)/2$ between the endpoints is defined as the distance measure between two matched line segments (Figure 4-2).

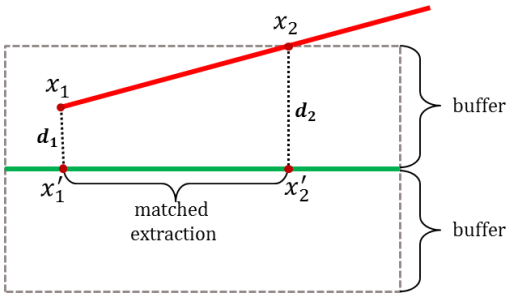

Figure 4-2 Matching line segment

4.2 Results and Evaluation

In this section, evaluation of the extracted road network is carried out based on the quality metrics discussed previously. First, the results for semi-automated road network extraction (RNE) algorithm that is driven by manually selected training data are presented. Then, results for the automated RNE algorithm that is driven by automatically generated training data are presented.

4.2.1 Evaluation of Semi-automated RNE algorithm

Table 4-1 provides an overview of the evaluation results of the road network extraction from the IKONOS test images (1-m spatial resolution, 512 by 512 pixels). The results are evaluated for the buffer zone size of 5 pixels. Therefore, maximum value of RMSE is 5 pixels. The evaluation results before and after the MRF post-processing stage in network formation step is displayed separately. The results show that applying a post-processing step to detect T-shape junctions leads to a significant increase in completeness. For the final results, the completeness and the correctness value are both above 90%. This is equivalent to saying that most of the road network is detected with a low false alarm rate.

Table 4-1 Quality assessment of Semi-automated RNE algorithm

	Before Post-processing				After Post-processing			
	Comp.	**Corr.**	**Qual.**	**RMSE**	**Comp.**	**Corr.**	**Qual.**	**RMSE**
Img1	0.8825	0.9231	0.8221	1.0012	0.9394	0.9091	0.8587	1.0365
Img2	0.8624	0.9718	0.8413	1.0800	0.9232	0.9720	0.8992	1.0793
Img3	0.9438	0.9932	0.9378	1.0016	0.9810	0.9904	0. 9717	1.0153

RMSE values are around 1 pixel. In other words, the average distance between the detected road network and the reference road network is approximately 1-meter (for 1-m resolution image). It represents the positional inaccuracy of extracted networks. This inaccuracy is mainly due to the template matching filter used in road class refinement step. The filter has a straightening effect on the curved roads. Therefore, the road centerline points are diverged from actual road centerlines. Another factor affecting the RMSE is occlusions on the road surface caused by trees, buildings, etc.

Figure 4-3 Semi-automated system: evaluation results for Test Image 1 (Green – correct extraction, red – missed roads, blue – false extraction).

The evaluation result of the image is depicted in Figure 4-3, where the green lines indicate lines that have been correctly extracted and the red lines indicate lines that have been missed. The major problem with the extracted road network from test image -1, as shown in Figure 4-3, is the falsely detected road segments. The main reason causing this problem is the misclassification of roads and other spectral similar object. If these misclassified regions also have a similar structural property with roads, then they won't be removed by template matching filter. As a result, they will appear on final road network.

There is another problem which is observed where the roads have sharp turns. As can be seen in Figure 4-4 road has made a shortcut instead of a sharp turn. This is due to a problem associated with the algorithm that we used to generate road segments. Since our road network is composed of small straight line segments connecting cluster centroids, positional accuracy of road network is low. Another reason causing this problem, as mentioned before, is the smoothing effect of Template Matching Filter used in road class refinement step.

Figure 4-4 Sharp turn: Extracted road (blue), Reference road (green), Cluster Centroids (red)

Figure 4-5 illustrates the result of the evaluation performances of the test image - 2. The extracted road network has very high completeness and correctness. Most of the roads have been extracted with a satisfactory accuracy. Some of the missing roads are due to the fact that these regions are not classified as road by classification algorithm. A close examination of these misclassified regions indicates that the spectral signature of these roads is slightly different than the rest of the roads due to the dust on their surfaces. Since these regions are not represented in the training data, they are not classified correctly. This problem can be solved by updating training set. The previously mentioned problem related to the sharp curved roads is also observed in this image in a couple of places.

Figure 4-5 Semi-automated system: evaluation results for Test Image 2 (Green – correct extraction, red – missed roads, blue – false extraction).

Figure 4-6 illustrates the result of the evaluation of the Test Image 3. It has the best performance among the examined images. The completeness of the extracted road network is 97% and its correctness is 99%.

Figure 4-6 Semi-automated system: evaluation results for Test Image 3 (Green – correct extraction, red – missed roads, blue – false extraction).

Table 4-1 provides an overview of the evaluation results of the extracted road junctions. The low completeness performance in image 1 and 2 is mainly due the junctions missed at the image boundaries, since the small road segments residing close to the image boundaries are removed by template matching filter. The correctness value of Test Image 1 is relatively lower because of false detected road segments.

Table 4-2 Quality assessment of extracted road junctions (Semi-automated system)

	Completeness	Correctness	Quality	RMSE
Test Image -1	0.8125	0.7778	0.6594	3.5993
Test Image -2	0.7727	1.0000	0.7727	1.9251
Test Image -3	1.0000	1.0000	1.0000	2.6110

4.2.2 Evaluation of Automated RNE algorithm

In order to automate the process of seed point selection, ACE algorithm has been employed. OC-SVM classifier trained on the generated seed points and road class model is obtained without any supervision of human operator.

Table 4-3 summarizes the evaluation results of our automatically extracted road networks from the same test images used in Semi-automated extraction system. The corresponding evaluation output images are shown in Figure 4-8, Figure 4-10 and Figure 4-12.

Table 4-3 Quality Assessment of Automated RNE algorithm

	Completeness	Correctness	Quality	RMSE (buffer width = 5)
Test image -1	0.6816	0.9894	0.6767	1.0596
Test image -2	0.8977	0.9177	0.8308	1.1921
Test image -3	0.9728	0.9430	0.9188	1.0895

The correctness and RMSE values are similar to the results of semi-automated system which was given previously in Table 4-1. However, the extracted road network by automated system has relatively lower completeness. Reduction in completeness value can be explained by the ACE algorithm's inability to find suitable seed centerlines, which causes a reduction in the performance of classification.

Figure 4-7.b shows the seed centerline points obtained by ACE algorithms. Most of the road centerlines are missing. This is mainly due to the irregularities on the road edges and the gradient constraint introduced by ACE algorithm not being satisfied for most of the roads for this particular image. As results, only a few pixels are available for training.

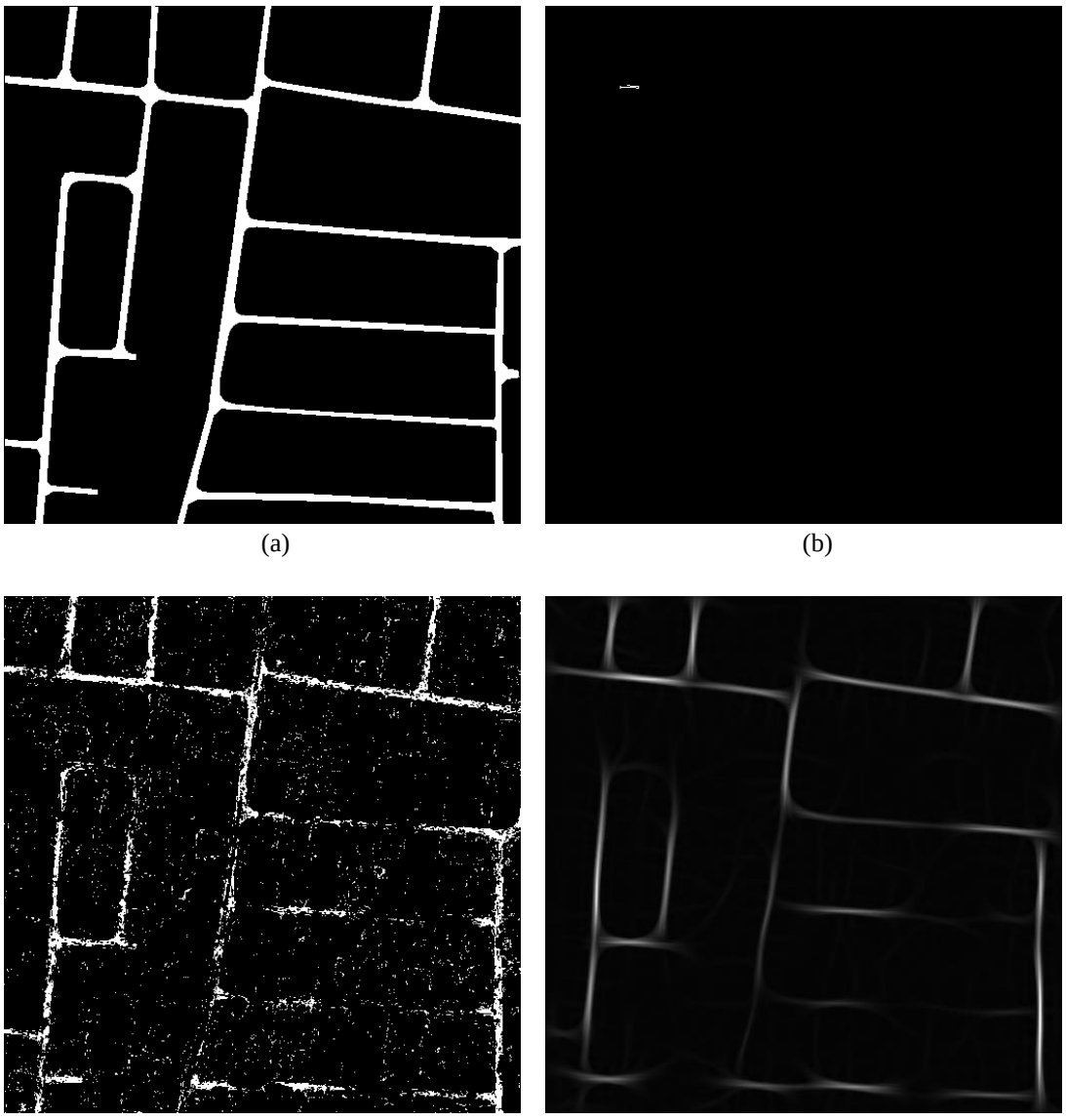

(a) (b)

(c) (d)

Figure 4-7 Self-supervised Classification output of Test Image 1: (a) Ground truth, (b) Seed points generated by ACE, (c) Classification output, (d) Template Matching Filter output.

Figure 4-8 Automated system: evaluation results for Test Image 1 (Green – correct extraction, red – missed roads, blue – false extraction).

Figure 4-8 illustrates the result of the evaluation of Test Image 1. When compared to the semi-automated system results, the completeness is decreased significantly. Approximately one third of the roads are missed.

The seed point extraction results for Test Image 2 are illustrated in Figure 4-9.b. Some of the detected centerline points do not belong to actual roads. These falsely detected centerlines cause misclassification problem (Figure 4-9.c). A majority of these misclassified regions are removed by template matching filter (Figure 4-9.d). The evaluation result of Test Image 2 is presented in Figure 4-10. Some problems observed on the image boundaries are due to the fact that filter characteristics are not well defined on these regions. The false detected segment shown in Figure 4-10 (marked with a yellow circle) is a dirt road and it is not included in the reference road map.

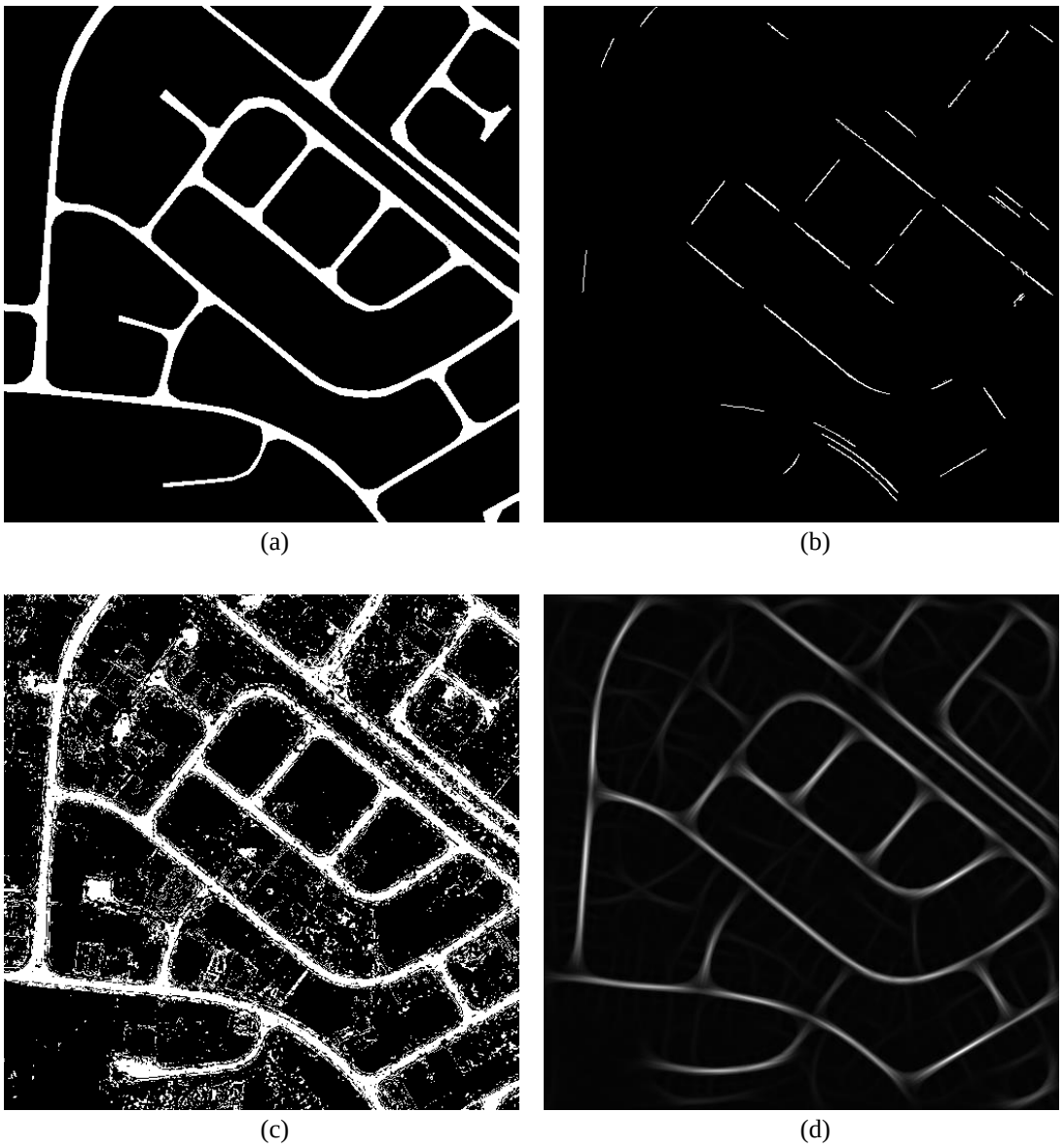

Figure 4-9 Self-supervised Classification output of Test Image 2: (a) Ground truth, (b) Seed points generated by ACE, (c) Classification output, (d) Template Matching Filter output.

Figure 4-10 Automated system: evaluation results for test image – 2 (Green – correct extraction, red – missed roads, blue – false extraction).

The classification output of Test Image 3 is presented in Figure 4-11.c. It is also noisy because of the false detected seed points. Although Template matching filter is removed most of the noises and open areas, some of the false classified regions which have elongated shape are remained. Figure 4-12 shows evaluation results of detected road network. Results are close to semi-automated system's result. However, there are some false positive extractions (blue lines). The false roads marked with a yellow circle can be eliminated by further analyzing network, since they are not connected to the rest of the road network.

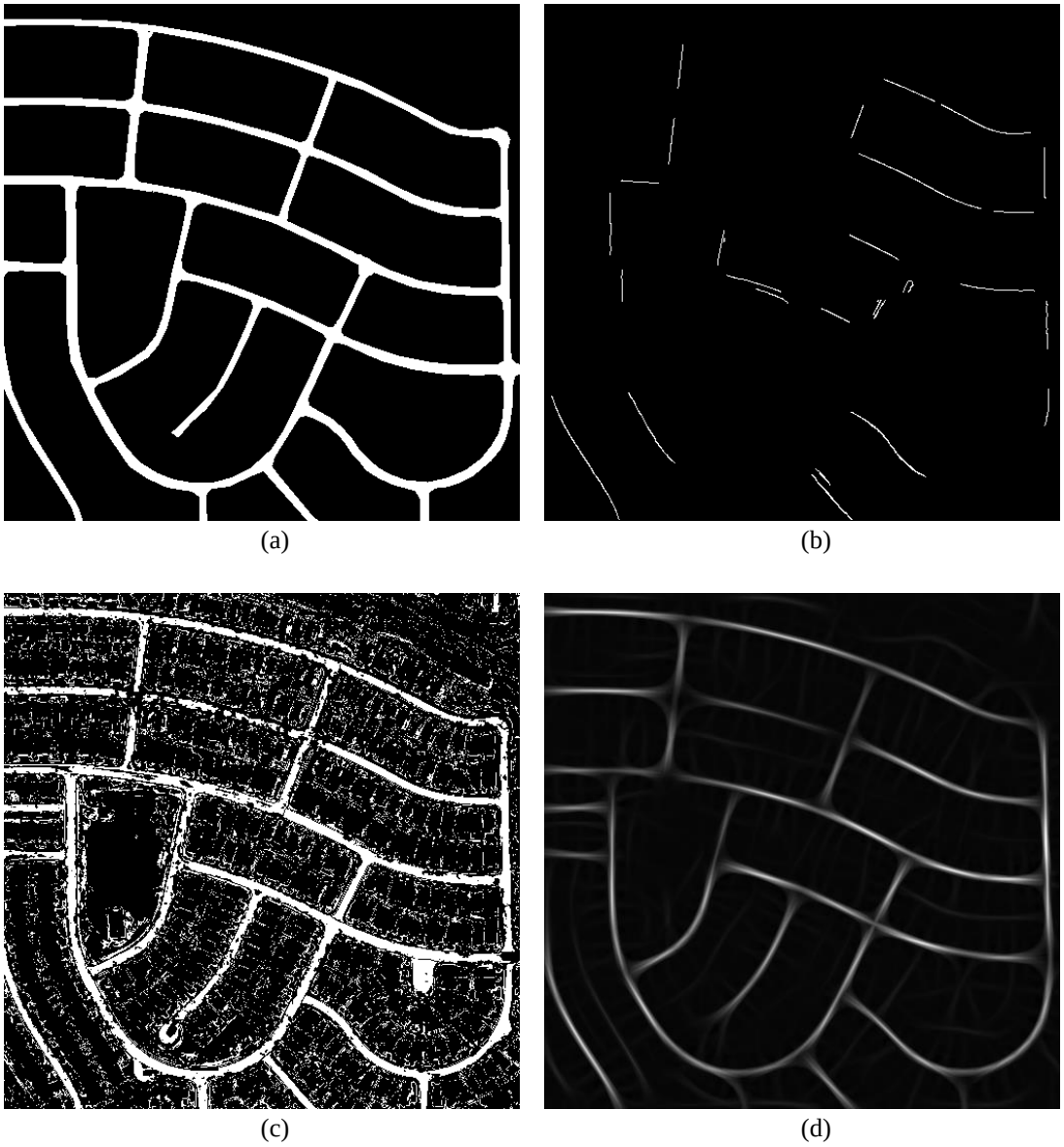

Figure 4-11 Self-supervised Classification output of Test Image 3: (a) Ground truth, (b) Seed points generated by ACE, (c) Classification output, (d) Template Matching Filter output.

Figure 4-12 Automated system: evaluation results for Test Image 3 (Green – correct extraction, red – missed roads, blue – false extraction).

Table 4-3 summarizes the evaluation results of the extracted road junctions. Junction detection performance of Test Image 2 and 3 is reduced slightly. However, for Test Image 1 only one third of the junctions can be detected.

Table 4-4 Quality assessment of extracted road junctions (Automated system)

	Completeness	Correctness	Quality	RMSE (buffer width = 5)
Test Image 1	0.3125	0.8333	0.2941	2.4979
Test Image 2	0.7727	1.0000	0.7727	2.9842
Test Image 3	1.0000	0.9524	0.9524	2.6946

4.2.3 MST-based Linking Algorithm for RNE

Doucette et al. present an approach to road extraction in classified imagery using self-organized road mapping (SORM) algorithm, combining a straight K-medians spatial clustering approach with a post-convergence node linking minimum spanning tree (MST) algorithm. In this thesis, cluster centroids derived by K-medians algorithm are connected with a MRF-based network topology extraction approach instead of the MST-based which is proposed in the original SORM algorithm.

In order to compare two approaches, a Minimum Spanning Tree (MST) is created by connecting the cluster centroids. A score is assigned to each link, which is based on the inter-cluster connection strength and cluster elongation. The resulting road networks for Test Images 1, 2 and 3 is displayed in

Figure 4-13, Figure 4-14 and Figure 4-15 respectively.

Since the MST is a single-linkage tree structure, closed loops are not possible which might result in valid links being discarded. Some invalid connections are also generated just to complete graph. These problems can be eliminated by adding a post-processing stage. Apart from these problems, as can be seen from these figures, MST-based approach is not very good at detecting road junctions. MRF-based node linking approach has better results than MST-based.

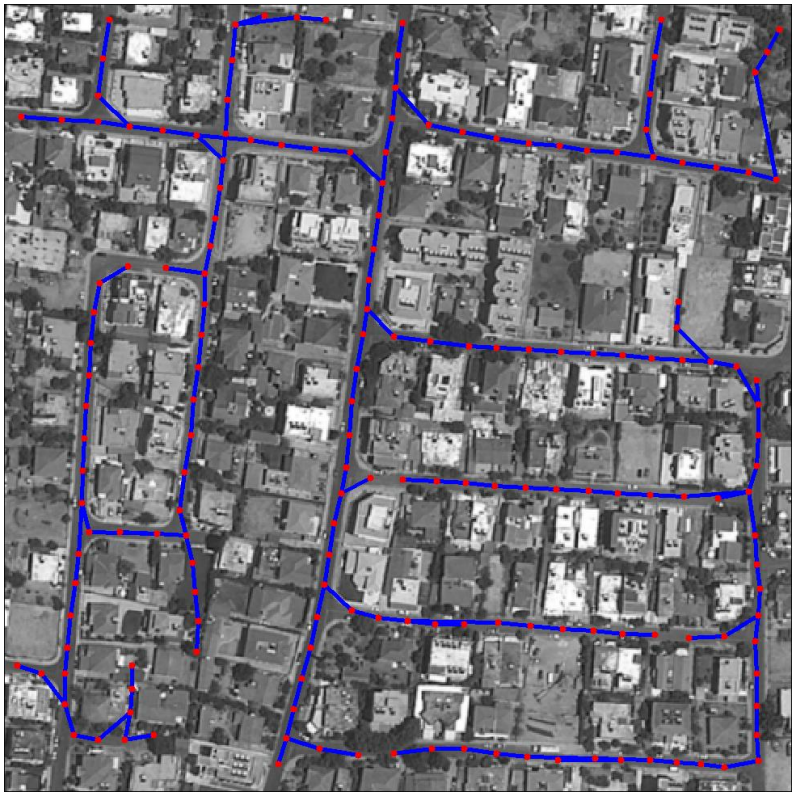

Figure 4-13 MST linking result of Test Image 1

Figure 4-14 MST linking result of Test Image 2

Figure 4-15 MST linking result of Test Image 3

4.3 Summary

In this chapter, evaluation results of the proposed semi-automated and automated RNE systems are presented. First, the evaluation results of semi-automated system are analyzed. In semi-automated system, seed points selected manually from different part of the road network so that the spectral signature of road can be modeled better. In order to improve the classification accuracy the training set selection procedure can be performed iteratively by monitoring the output of classification. If the some of the roads are not detected in classification, the operator may update the training set and rerun the training.

Automating the process of training set selection procedure seems to be reducing the ratings. This is mainly due to the fact that ACE algorithm is not very promising to detect centerline points. The false detected centerline points or some missing centerline points degrade the classification results and this directly has a negative impact on the final road network.

Template matching filter is very useful in removing open areas which have similar spectral signature with roads. It also removes the irregularities on road boundaries and small noisy regions and furthermore it fills the occluded regions on the road surface caused by shadows, trees, buildings, etc. On the other hand, it has some negative effects, like smoothing the road curves which reduces the positional accuracy of road network.

CHAPTER 5

CONCLUSION AND FUTURE WORK

5.1 Summary

In this study, a road network extraction framework is proposed. The study investigates to integrate a variety of algorithms within the road extraction system. In the first step, the spectral classification of input images is performed using two different classifiers: OC-SVM and GMM classifiers. Optimum parameter selection procedures for both classifiers are presented and a comparison of classification performances is provided. The effect of feature reduction technique called principal Component Analysis (PCA) on spectral classification results is also analyzed. The extracted road "potential image" which is indicate the probability of a pixel belong to road class is used as input to second step of the framework which is road class refinement step. In this step, our aim is to remove misclassified road for the purpose of increasing classification accuracy. In the third step, road centerline extraction procedure via K-Medians spatial clustering algorithm is explained. In the fourth and final step a MRF based road network construction algorithm is presented. Overall performance of both semi-automated and fully automated network extraction systems is evaluated quantitatively in Chapter 4 based on the quality metrics, completeness, correctness, quality and RMSE.

5.2 Discussion

It is shown that using original spectral band of the image in spectral classification is not very efficient due to high correlation between them. Instead, first and second principal components are used for spectral classifications. Experimental results show that the classification results are similar. However, by using the less number of features the classification time is reduced.

The spectral classification of roads generally gives satisfactory results whether OC-SVM or GMM is used. However, the performance of GMM classifier highly depends on the initial values of mixture parameters. A poor choice of initial parameters might invariably lead to poor results, as the Expectation Maximization (EM) algorithm converges only to a local optimization point. Therefore, some of experimental results obtained by GMM classifier are failed. As a result OC-SVM is a more robust classifier than GMM.

One of the major problems with the spectral classification of roads is the miss-classified regions due to the spectral similarity between roads and other objects such parking lots, buildings, crop fields, etc. These regions are eliminated by applying a Template matching filter. Template matching filter improves the classification accuracy not only by removing non-road regions but also by filling small gaps on road network. It also removes irregularities on road boundaries which leads to a better localization of road centerline points. However, there are some problems observed with Template matching filter. Since it favors the long straight roads, it smoothes the curvy roads. Therefore, the geometrical accuracy of road network are become poorer on locations where roads make turn.

The MRF based road network extraction framework proposed by Tupin et al. is successfully adapted to our problem. However it misses the majority of T-shape junctions. It is due to the fact that the original energy function of MRF favors long roads against intersections. In order to detect junction points properly a modification on the energy function is proposed. With the new energy function, extracted road network re-analyzed to detect missed road junctions. Almost all the junctions are detected with this post-processing stage.

Performance evaluation of the final road network has been assessed based on road network extraction results obtained on a set of test images. The measures used to evaluate the algorithm performance are completeness, correctness, quality and RMSE. The Semi-automated algorithm is able to consistently extract 85% to 90% of the road network and has a high performance against all the three measures, completeness, correctness and accuracy, which demonstrates the robustness of the proposed road extraction system. Fully automated algorithm has lower completeness values compared to semi-automated system. This result is due to the ACE algorithm's inability to find suitable seed centerlines and also false detected centerlines.

Overall road network extraction procedure takes very long time to complete (approximately 15 min for 512 by 512 image in a PC with 3.2GHz 8-core Intel i7 processor). Most of time is spent by stochastic optimization stage with Simulated Annealing. Using ICM which is a deterministic optimization technique instead of Simulated Annealing significantly reduces the total computational time. However, ICM only reaches local optimum point rather than global. Most of the algorithms are implemented using MATLAB®. It is expected that the total computational time can be greatly reduced if all the algorithms were implemented in C/C++.

5.3 Future Work

There are several areas where the extraction quality could be improved. For example, in the current implementation, only very simple junctions can be detected. It is necessary to use a more sophisticated junction model especially for urban roads.

Since the seed centerline points extracted by ACE are not very reliable for some images, the classification performance of the proposed automated system can be poor. Therefore, the road model used by ACE needs to be improved to eliminate false detected centerline points.

Another way of improving the completeness could be an additional step of closing further gaps after the final network extracted. One possibility is to run a road tracking algorithm starting from the endpoints of unconnected road segments and to find a reasonable path to the rest of the network.

In the network formation step, the road network is defined in terms of small straight line segments connecting cluster centroids which were obtained in road centerline extraction step. The geometric accuracy of the final network could be improved using curvy lines instead of straight lines. These lines can be obtained by a skeleton extraction technique applied on raw or filtered classified image. Further improvement on accuracy can be achieved by modifying the structure of Template matching so that it is more sensitive on curved roads. In a further improvement, the template matching filter idea can be merged the MRF clique potential function definition in order to obtain more powerful road model.

In the proposed algorithm, the roads overpassing other roads are not considered. These overpassing regions are detected as junction points in the final road network. For a complete road network topology, these regions also need to be considered. However, it is very changeling problem and relatively little research work has been done on this area.

REFERENCES

Besag, J. (1974). Spatial interaction and the statistical analysis of lattice. *J. R. Statist. Soc. B, vol. 36*, 192-326.

Besag, J. (1986). On the Statististical Analysis of Dirty Pictures. *J. R. Statist. Soc. B*, 48(3):259–302.

Černý, V. (1985). A thermodynamical approach to the travelling salesman problem: an efficient. *Journal of Optimization Theory and Applications*, 45:41-51.

Cortes, C., & Vapnik, V. N. (1995). Support-vector networks. *Machine Learning*, 20:273-297.

Doucette, P., Agouris , P., & Stefanidis, A. (2004). Automated road extraction from high resolution multispectral imagery. *Photogrammetric Engineering & Remote Sensing* , 70(12):1405-1416.

Doucette, P., Agouris, P., Stefanidis, A., & Musavi, M. (2001). Self-organized clustering for road extraction in classified imagery. *ISPRS Journal of Photogrammetry and Remote Sensing*, 55(5-6):347-358.

Geman, S., & Geman, D. (1984). Stochastic Relaxation, Gibbs Distribution, and Bayesian Restoration of Images. *IEEE Tran. on Pattern Analysis and Machine Intelligence, vol. 6*, 721-741.

Géraud, T., & Mouret, J. B. (2004). Fast road network extraction in satellite images using mathematical morphology and Markov random fields. *EURASIP Journal on applied signal processing, 2004*, 2503-2514.

Hammersley, J., & Clifford, P. (1971). Markov Fields on finite graphs and lattices. *Unpublished manuscript*.

Hinz, S., & Baumgartner, A. (2003). Automatic extraction of urban road networks from multi-view aerial imagery. *ISPRS J. Photogramm. 58(1-2)*, 83-98.

Hu, X., Tao, C. V., & Hu, Y. (2004). Automatic Road Extraction from Dense Urban Area by Integrated Processing of High Resolution Imagery and LIDAR Data. *Proceedings of ISPRS XXth Congress, Istanbul, Turkey, July 12-23*, (CDROM).

Katartzis, A., Sahli, H., Pizurica, V., & Cornelis, J. (2001). A model-based approach to the automatic extraction of linear features from airborne images. *Geoscience and Remote Sensing, IEEE Transactions on, 39(9)*, 2073-2079.

Kirkpatrick, S., Gelatt Jr., C. D., & Vecchi, M. P. (1983). Optimization by Simulated Annealing. . *Science*, 220(4598):671–680.

Kohonen, T. (2001). Self-Organizing Maps. *Springer-Verlag*.

Lacoste, C., Descombes, X., & Zerubia, J. (2005). Point processes for unsupervised line network extraction in remote sensing. Pattern Analysis and Machine Intelligence. *Pattern Analysis and Machine Intelligence, IEEE Transactions on, 27(10)*, 1568-1579.

Mena, J. B. (2003). State of the art on automatic road extraction for GIS update: a novel classification. *Pattern Recognition Letters, 24(2003)*, 3037-3058.

Mena, J. B., & Malpica, J. A. (2005). An automatic method for road extraction in rural and semi-urban areas starting from high resolution satellite imagery. *Pattern Recognition Letters 26(9)*, 83-98.

Ready, P. J., & Wintz, P. A. (1973). Information extraction, SNR improvement and data compression in multi-spectral imagery. *IEEE Transactions on Communications, COLM-21, 10*, 1123-1130.

Schölkopf, B., Platt, J. C., Shawe-Taylor, J., Smola, A. J., & Williamson, R. C. (1999). Estimating the support of a high-dimensional distribution. *Technical report, Microsoft Research*, MSR-TR-99-87.

Song, M., & Civco, D. (2004). Road network extraction using SVM and image segmentation . *Photogrammetric Engineering & Remote Sensing*, 70:1365-1371.

Stoica, R., Descombes, X., & Zerubia, J. (2004). A Gibbs point process for road extraction from remotely sensed images. *International Journal of Computer Vision, 57(2)*, 121-136.

Tupin, F., Maitre, H., Mangin, J. -F., Nicolas, J. -M., & Pechersky, E. (1998). Detection of linear features in SAR images: application to road network extraction. *IEEE Transactions on Geoscience and Remote Sensing, vol. 36, no.2* , 434-453.

Wiedemann, C. (2003). External evaluation of road networks. *ISPRS Archives, Vol. XXXIV, Part 3/W8, Munich, September 17-19*.

Zhang, C. (2004). Towards an operational system for automated updating of road databases by integration of imagery and geodata. *ISPRS Journal of Photogrammetry & Remote Sensing, 58*, 166-186.

APPENDIX A

EVALUATION RESULTS OF IKONOS TEST IMAGES

Table A-1 Performance evaluation of extracted road network (IKONOS test images, 1000 by 1000 pixels)

Image	Completeness	Correctness	Quality
1	0.3851	0.3747	0.2344
2	0.3208	0.7359	0.2877
3	0.2875	0.7191	0.2585
4	0.6134	0.2943	0.2483
5	0.6103	0.6020	0.4349
6	0.5586	0.6775	0.4413
7	0.7272	0.9016	0.6737
8	0.5229	0.7139	0.4323
9	0.4073	0.8811	0.3861
10	0.5687	0.7092	0.4611
Mean	**0.5002**	**0.6609**	**0.3858**
Std. Dev.	**0.1431**	**0.1945**	**0.1349**

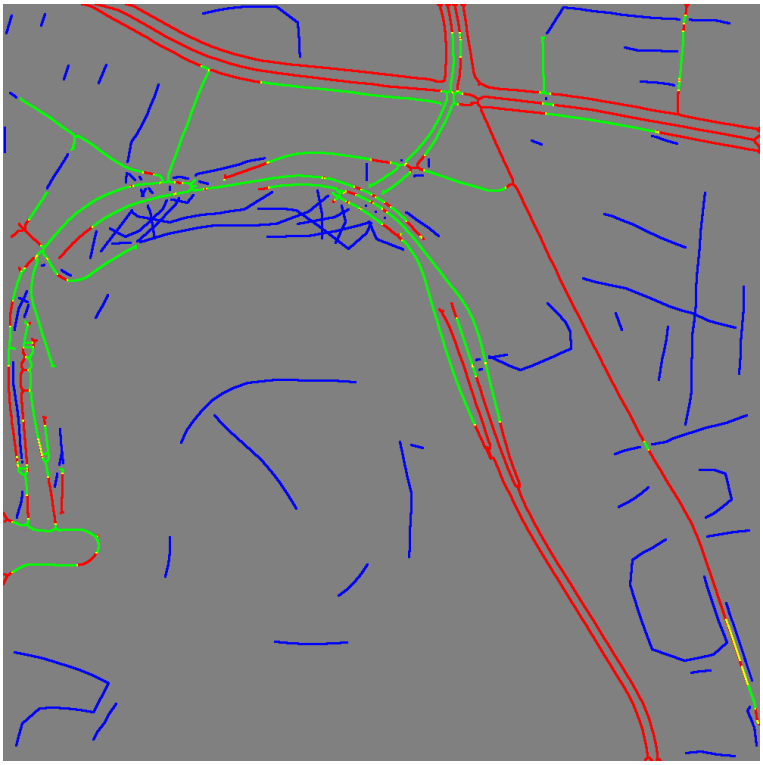

Figure A-1 Evaluation Results for IKONOS Test Image 1: Green – correct extraction, red – missed extraction, blue – false extraction

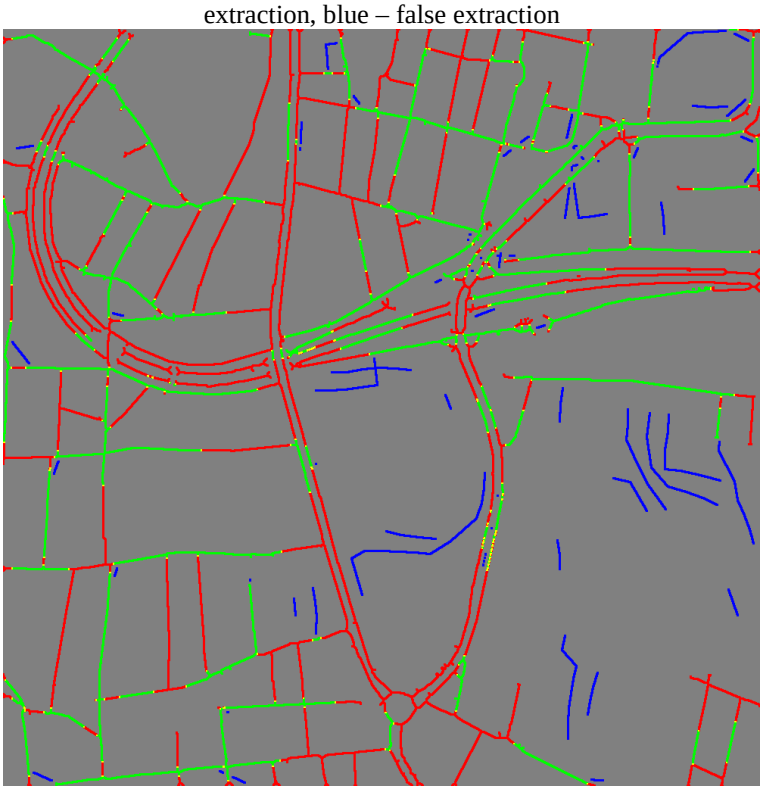

Figure A-2 Evaluation Results for IKONOS Test Image 1: Green – correct extraction, red – missed extraction, blue – false extraction

Figure A-3 Evaluation Results for IKONOS Test Image 3: Green – correct extraction, red – missed extraction, blue – false extraction

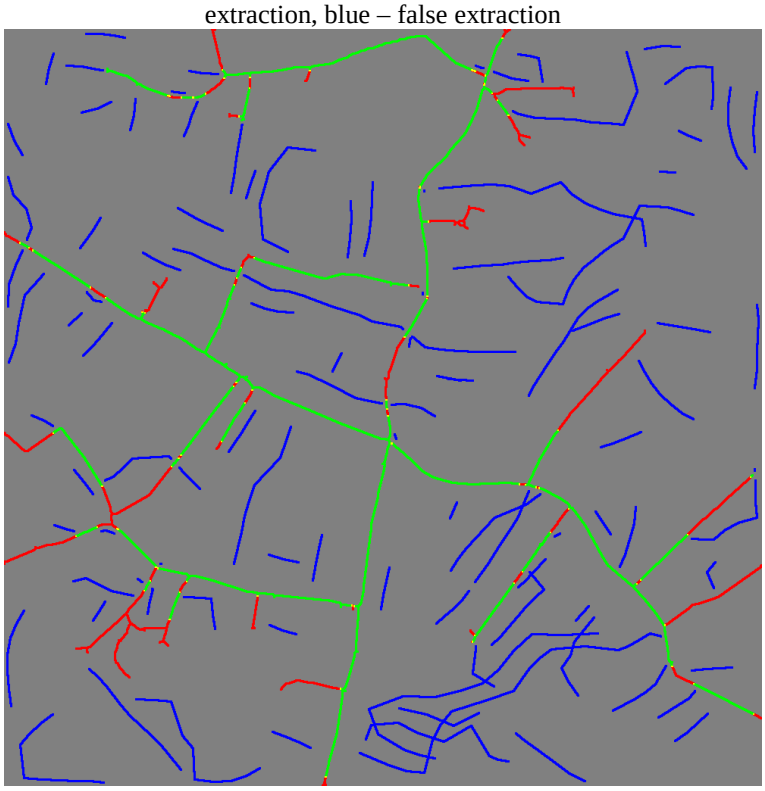

Figure A-4 Evaluation Results for IKONOS Test Image 4: Green – correct extraction, red – missed extraction, blue – false extraction

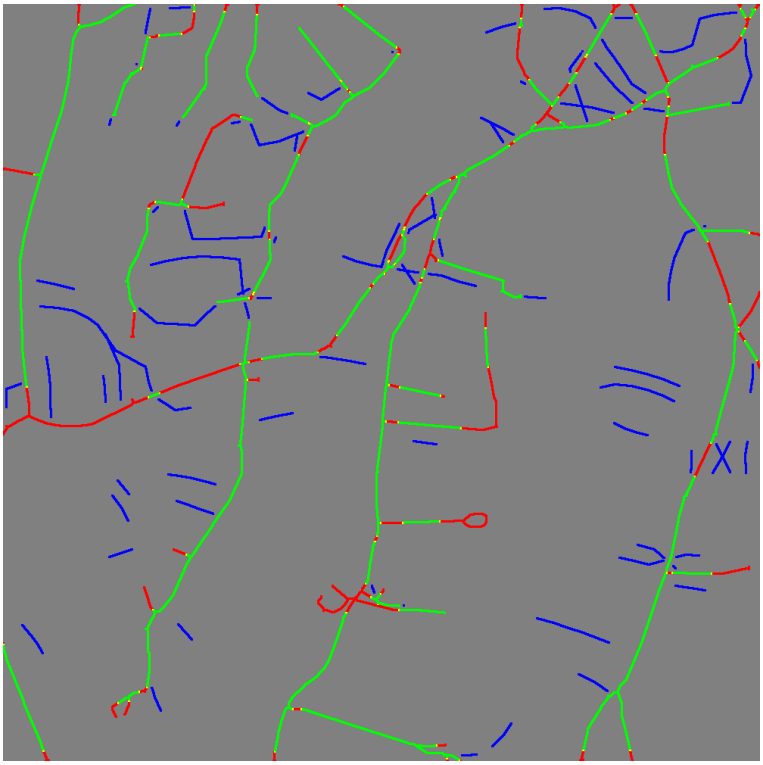

Figure A-5 Evaluation Results for IKONOS Test Image 5: Green – correct extraction, red – missed extraction, blue – false extraction

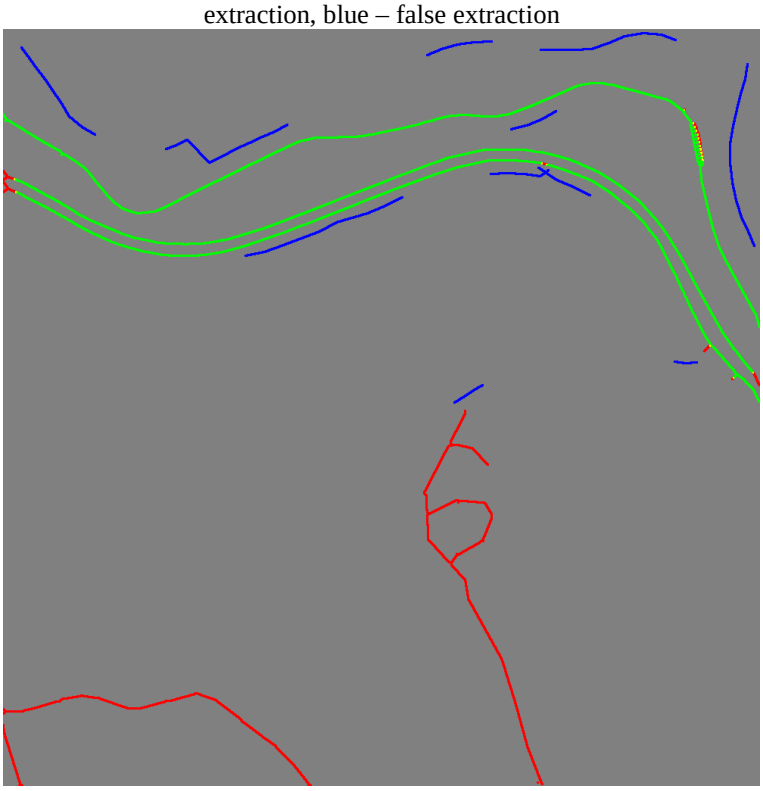

Figure A-6 Evaluation Results for IKONOS Test Image 6: Green – correct extraction, red – missed extraction, blue – false extraction

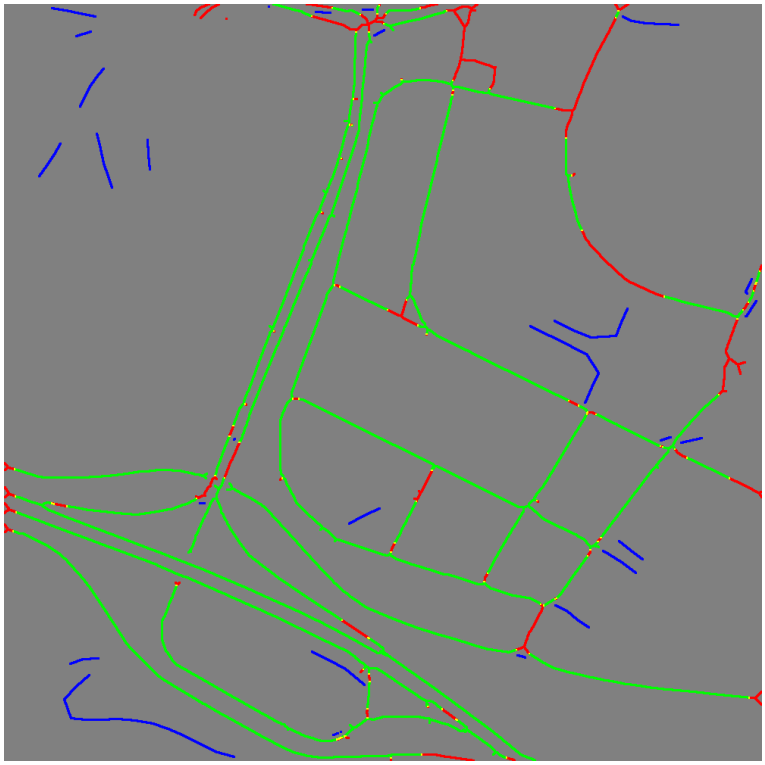

Figure A-7 Evaluation Results for IKONOS Test Image 7: Green – correct extraction, red – missed extraction, blue – false extraction

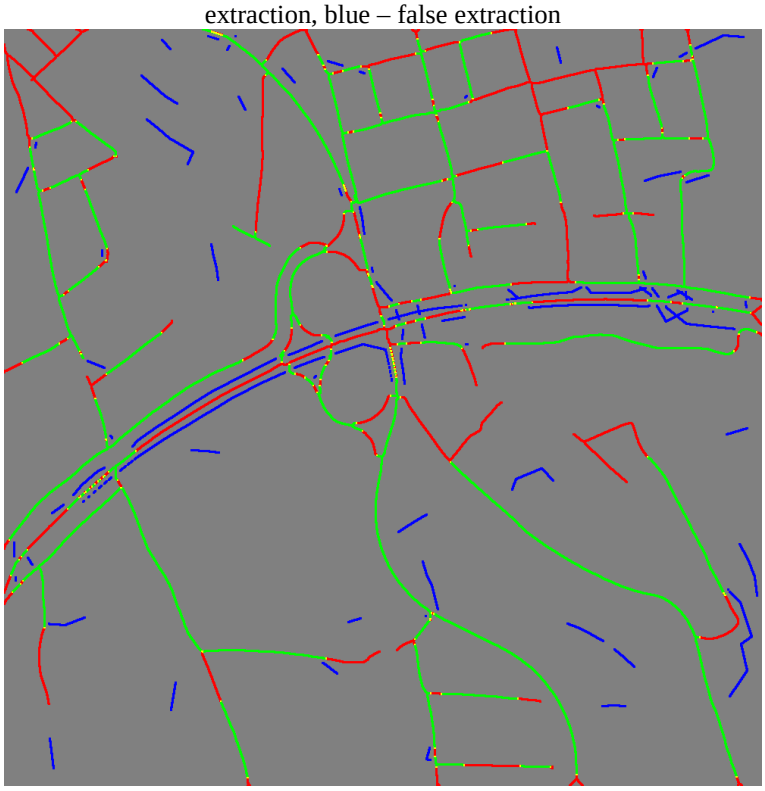

Figure A-8 Evaluation Results for IKONOS Test Image 8: Green – correct extraction, red – missed extraction, blue – false extraction

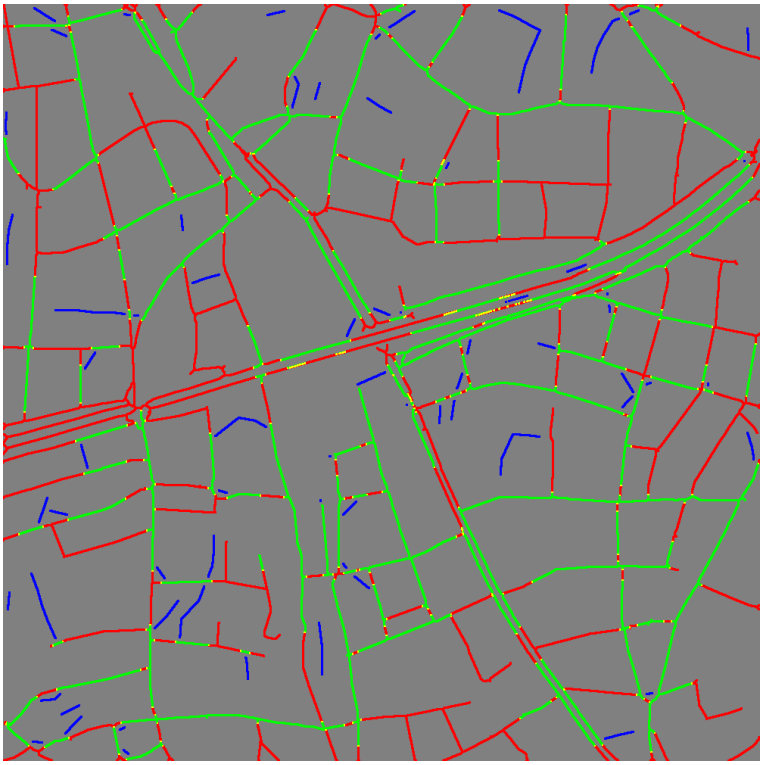

Figure A-9 Evaluation Results for IKONOS Test Image 9: Green – correct extraction, red – missed extraction, blue – false extraction

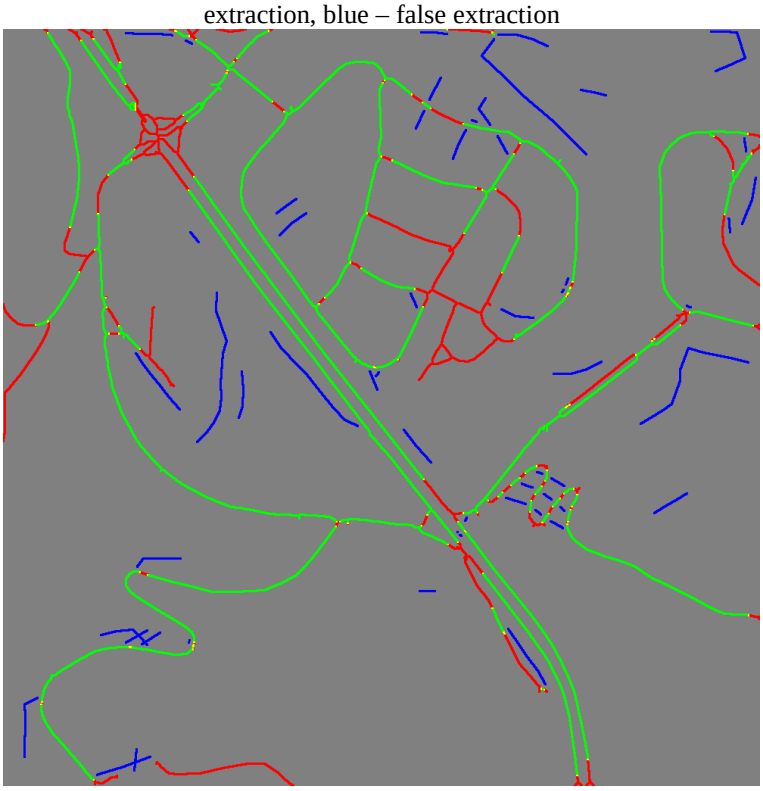

Figure A-10 Evaluation Results for IKONOS Test Image 10: Green – correct extraction, red – missed extraction, blue – false extraction